Dynamic regulation of NAT10-mediated mRNA acetylation at synapses by learning and memory in mouse hippocampus

Hai-Qian Zhou[1,2#], Jia-Wei Zhang[1#], Zhen Zhu[1#], Wei-Peng Lin[1,2#], Hao-JY Jin[1], Yang-Yang Ding[1], Dong-Sheng Chen[3*] and Dong-Min Yin[1,2,4,5*]

1 Key Laboratory of Brain Functional Genomics, Ministry of Education and Shanghai, School of Life Science, East China Normal University, Shanghai, 200062, China

2 Joint Center for Translational Medicine, Shanghai Fifth People's Hospital, Fudan University and School of Life Science, East China Normal University, Shanghai, 200240, China

3 State Key Laboratory of Common Mechanism Research for Major Diseases, Suzhou Institute of Systems Medicine, Chinese Academy of Medical Sciences & Peking Union Medical College, Suzhou, 215123, China

4 NYU-ECNU Institute of Brain and Cognitive Science at NYU Shanghai, Shanghai, 200062, China.

5 Lead contact

[#]H-Q Z, J-W Z, Z Z and W-P L contributed equally to this work.

[*]Correspondence should be addressed to Prof. Dong-Sheng Chen,

Tel: 86-512-62873780

Fax: 86-512-62873779

Email: cds@ism.pumc.edu.cn

or

Prof. Dong-Min Yin,

Tel: 86-21-62232016

Fax: 86-21-62601953

Email: dmyin@brain.ecnu.edu.cn

Abstract

Post-transcriptional modification of RNA plays important roles in regulating brain functions including learning and memory. N4-acetylcytidine (ac4C), the only known form of RNA acetylation in eukaryotes, has recently been shown to regulate mRNA stability and translation efficiency. However, the function and regulation of mRNA acetylation in the brain remain largely unknown. Here we performed ac4C dot-blots, liquid chromatography tandem mass spectrometry (LC-MS/MS), and ac4C-RNA immunoprecipitation followed by next-generation sequencing (acRIP-seq) to investigate the dynamic change of ac4C mRNA in mouse hippocampus during learning and memory. This study focused on Morris water maze (MWM), a behavioral protocol commonly used for studying hippocampus-dependent spatial learning and memory. Interestingly, the levels of ac4C mRNA were upregulated in the synaptosomes (SYN) after memory formation but returned to normal levels after memories were naturally forgotten. The protein levels of N-acetyltransferase 10 (NAT10), the ac4C writer, were also increased in the SYN after memory formation and returned to control levels after memory forgetting. Strikingly, genetic ablation of Nat10 from hippocampal neurons significantly reduced the ac4C modification of Arc, Camk2α and Grin2b mRNA and their protein levels in the SYN of training mice, which was accompanied by deficits in synaptic plasticity and behaviors of learning and memory. These results demonstrate the dynamics and roles of synaptic mRNA acetylation in learning and memory, offering insights into the epitranscriptomic regulation of brain functions. The dataset of ac4C mRNA from mouse hippocampus is accessible via the website (http://ac4catlas.com/).

Introduction

Precise regulation of protein synthesis at the right place and right time is important for various brain functions including learning and memory (Besse and Ephrussi, 2008; Shrestha and Klann, 2022). For instance, local protein synthesis near stimulated synapses plays critical roles in synaptic plasticity and memory consolidation(Martin et al., 2000; Sutton and Schuman, 2006). Mechanistically, epigenetic regulations on DNA and histone proteins have been widely studied in the context of learning and memory (Day and Sweatt, 2011; Levenson and Sweatt, 2005). However, the roles of chemical modifications on mRNA in learning and memory have only become appreciated in recent years (Fischer et al., 2007; Kouzarides, 2007; Levenson et al., 2004). Especially, N6-methyladenosine (m6A), a well-studied form of mRNA methylation has been shown to regulate synaptic plasticity as well as learning and memory (Merkurjev et al., 2018; Shi et al., 2018; Zhuang et al., 2023).

N4-acetylcytidine (ac4C) is the only known form of RNA acetylation in eukaryotes (Boccaletto et al., 2018). Initially, ac4C was identified in the transfer RNA (tRNA) (Kowalski et al., 1971; Kruppa and Zachau, 1972; Oashi et al., 1972; Stern and LH, 1978). Later studies revealed that ac4C also occurred in the 18S ribosomal RNA (rRNA) (Ito et al., 2014a). More recently, ac4C has been found in mRNA from mammalian cells, where it has been shown to promote mRNA stability and translational efficiency (Arango et al., 2018; Arango et al., 2022). N-acetyltransferase 10 (NAT 10) is the only known ac4C writer in mammalian cells (Ito et al., 2014b). NAT10-mediated mRNA acetylation has been reported to regulate tumorigenesis (Liu et al., 2023b; Wang et al., 2022), stem cell differentiation (Hu et al., 2024a), cardiac remodeling (Shi et al., 2023a), germ cell maturation (Jiang et al., 2023) and pain signaling in the spinal cord (Xu et al., 2023; Zhang et al., 2023a). However, the function and regulatory mechanisms of mRNA acetylation in the brain remain poorly understood.

The hippocampus plays an important role in learning and memory (Jarrard, 1993). Pyramidal neurons in the CA3 region of hippocampus establish direct projection to CA1 pyramidal neurons through the Schaffer collateral (SC) pathway, known as the SC-CA1

synapse. The glutamatergic transmission at SC-CA1 synapses was found to be enhanced following training in the MWM (Moser et al., 1994), a behavioral paradigm for learning and memory (Morris, 1984). Long-term potentiation (LTP), a widely-studied form of synaptic plasticity in hippocampus, is most closely linked to learning and memory (Bliss and Collingridge, 1993). Several studies showed that mRNAs and ribosomes were present in the synaptosomes, contributing to protein synthesis at synapses (Biever et al., 2020). In principle, neural activities can regulate local protein synthesis through post-transcriptional modification of synaptic mRNAs (Goldie and Cairns, 2012). However, whether synaptic mRNAs were subjected to NAT10-mediated acetylation and whether this process contributed to synaptic plasticity and memory remain elusive.

Given that eukaryotic mRNAs are polyadenylated, we first conducted ac4C dot-blots and liquid chromatography-tandem mass spectrometry (LC-MS/MS) analysis to examine the acetylation of polyadenylated (polyA) RNA from mouse hippocampus during and after training in the MWM. Our findings revealed that the acetylation of polyA RNA was increased in the synaptosomes (SYN), rather than in the homogenates (HOM), following memory formation, and subsequently returned to baseline after memory forgetting. The dynamic changes of mRNA acetylation at synapses throughout the processes of learning and memory was further demonstrated by ac4C-RNA immunoprecipitation followed by next-generation sequencing (acRIP-seq). Moreover, the increased levels of ac4C mRNA in the SYN after learning and memory were accompanied with the increased protein levels of NAT10 at synapses. Genetic ablation of Nat10 from hippocampal neurons in adult mice using the Cre/Loxp strategy significantly reduced the acetylation of Arc, Camk2α and Grin2b mRNA and their protein levels at synapses, and thus impaired learning and memory in the MWM. Collectively these results demonstrate the dynamic regulation of NAT10-mediated acetylation of synaptic mRNAs during learning and memory. The dataset of ac4C epitranscriptome from mouse hippocampus is freely accessible at the website (http://ac4catlas.com/).

Results

Presence of ac4C modification of polyA RNA in mouse hippocampus

Recent studies raised the debate about the presence of ac4C in mRNA from mammalian cells (Beiki et al., 2024; Georgeson and Schwartz, 2024). We first investigate whether ac4C is a detectable modification of mRNA from mouse hippocampus. To this end, we first purified polyA RNA from the HOM of mouse hippocampus and determine their ac4C levels using LC-MS/MS. The purity of polyA RNA was verified by the bioanalyzer analysis (Figure 1A and 1B) and dramatic reduction of 18S rRNA relative to total RNA in reverse transcription followed by quantitative PCR (RT-qPCR) (Figure 1C). An ac4C standard curve was generated to calculate the stoichiometry levels of ac4C in polyA RNA samples (Figure 1D). Both the ac4C and m6A peaks can be detected by the chromatograms in the standard samples but not in the blank solution (Figure 1E and 1F). The polyA RNA purified from the HOM of mouse hippocampus showed ac4C peaks with a stoichiometry level of 0.426 ± 0.049% (n = 3 biological replicates) (Figure 1G and 1H). Likewise, the polyA RNA purified from the HOM of mouse hippocampus showed m6A peaks with a stoichiometry level of 0.173 ± 0.018% (n = 3 biological replicates) (Figure 1G and 1I), which is consistent with the previous study form mouse brain (Li et al., 2023). When the polyA RNA samples were incubated with 50 mM NH_2OH for 1 h before LC-MS/MS, a protocol of chemical deacetylation of ac4C (Sinclair et al., 2017), the stoichiometry levels of ac4C were significantly reduced (Figure 1H), indicating the validity of the LC-MS/MS analysis. By contrast, the stoichiometry levels of m6A in polyA RNA samples remained unchanged after NH_2OH treatment (Figure 1I), supporting the specificity of the deacetylation method. Altogether these results demonstrate the presence of ac4C modification in polyA RNA from mouse hippocampus. Given that polyA RNA consists of mRNA and long noncoding RNA (lncRNA) (Yu et al., 2020), we further performed acRIP-seq to analyze the ac4C mRNAs in mouse hippocampus (see below).

Characterization of ac4C mRNA in the HOM of mouse hippocampus after learning and memory

We used the behavioral protocol of MWM (Vorhees and Williams, 2006) to study how learning and memory regulate mRNA acetylation in mouse hippocampus. The control mice were placed in the MWM with a visible platform once a day for 2 days, and thus could reach the visible platform in the target region without training (Figure S1A and S1B). However, the control mice could not remember the target region during the probe test at day 6 (Figure S1A and S1C). In contrast, the learning mice were subjected to training in the MWM with a hidden platform (Figure S1D and S1E). The learning mice took 5 days of training to remember the target region during the probe test at day 6 (Figure S1E and S1F), indicative of memory formation. Consistent with the previous study (Hoz et al., 2004), the learning mice could not remember the target region during the probe test at day 20, i.e., after staying in home cage for 2 weeks without training (Figure S1D and S1G), indicating that memories were naturally forgotten (Figure S1H).

We next performed acRIP-seq (Arango *et al.*, 2018) to identify ac4C mRNA in the HOM of mouse hippocampus. Two libraries of RNA (acRIP and input) were subjected to the next-generation sequencing (NGS) for each sample (Table S1). The acRIP-seq reads were mapped to mouse hippocampal transcriptome to identify ac4C enriched regions relative to input, and the fold enrichment (FE) of an ac4C peak was defined as acRIP / input (Figure S2A). An ac4C peak was considered positive when its FE > 2 and P-value < 0.05 (Zhang et al., 2023b). When we analyzed the cumulative distribution curve of the levels of ac4C mRNA, the FE of ac4C mRNA was the sum of the FE of all ac4C peaks in one particular mRNA (see details in the Method).

We performed acRIP-seq for three HOM replicates from control and learning mice one hour after probe tests in the MWM (i.e., at day 6). The ac4C peak and ac4C mRNA identified in three biological replicates of control mice were largely overlapped (Figure S2B and S2C). Moreover, the acRIP-seq revealed the same consensus motif AGCAGCTG in the ac4C peak regions from three biological replicates of control mice (Figure S2D). These results indicate the consistency of the acRIP-seq for mouse hippocampus. The ac4C peak that were identified from at least two of the three biological replicates were considered reliable (Figure S2E and S2F). Only mRNAs

corresponding to these reliable ac4C peaks are defined as reliably ac4C mRNAs. We identified 14516 ac4C peaks and 8303 ac4C mRNAs from the HOM of control mice (Figure S2E and Table S2), and 13348 ac4C peaks and 8107 ac4C mRNAs from the HOM of learning mice (Figure S2F and Table S2). As a control of the acRIP-seq, only 1800 ac4C peaks were identified from the HOM of control mice when we performed IgG immunoprecipitation of RNA followed by NGS, indicating the specificity of acRIP-seq.

When we compared the transcripts with ac4C modifications to the entire transcriptome, we found that 49.22 ± 2.52% (n = 3 biological replicates) of the mRNAs in the mouse hippocampus were modified by ac4C. In line with the previous study from Hela cells (Arango et al., 2018), most ac4C peaks were identified in the coding sequence (CDS) of mRNA in mouse hippocampus (Figure S2G). On average, every acetylated transcript had 1.83 ± 0.05 (n = 3 biological replicates) ac4C peaks in mouse hippocampus. The numbers of ac4C peak per acetylated mRNA were comparable across three biological replicates and between control and learning mice (Figure S2H). Likewise, the ac4C dot-blots of polyA RNA, and the cumulative distribution of FE of ac4C mRNA in the HOM were similar between the control and learning mice (Figure S2I and S2J). The cumulative distribution of mRNA counts in the HOM that were revealed by the NGS of input RNA were also similar between control and learning mice (Figure S2K). Altogether these results suggest that the total levels of ac4C mRNA in the HOM of mouse hippocampus may not be altered by learning and memory in the MWM.

Dynamic change of ac4C polyA RNA in the SYN of mouse hippocampus during learning and memory in the MWM

We next purified the SYN fraction from mouse hippocampus, enriched for synaptic proteins (PSD95 and synapsin 1) and depleted of cytoplasm (the S2 fraction)-restricted protein (α-tubulin) (Figure 2A). We then analyzed the levels of ac4C polyA RNA purified from the SYN with the ac4C dot-blots. The control and learning mice showed similar levels of ac4C polyA RNA in the SYN at day 1 (Figure 2B). Strikingly, the

levels of ac4C polyA RNA showed a significant increase in the SYN of learning mice at day 6, compared with controls (Figure 2C). However, the levels of ac4C polyA RNA returned to control levels in the SYN of learning mice at day 20 (Figure 2D). These results suggest that acetylation of polyA RNA was upregulated in the SYN of mouse hippocampus during memory formation but returned to control levels after memory forgetting. The dynamic change of ac4C polyA RNA in the SYN of mouse hippocampus during learning and memory was verified by the assay of LC-MS/MS (Figure 2E).

Characterization of ac4C mRNA in the SYN of mouse hippocampus

Given that the amount of RNA from SYN (100 ng per mouse hippocampus) is much less than that from HOM (50 ug per mouse hippocampus), we used the protocol of low-input acRIP-seq to identify ac4C mRNA in the SYN (see details in the Methods). Due to the limited yield of SYN RNA, we purified the SYN RNA from the hippocampus of 10 adult mice and combined them into one sample. Each sample from control and learning mice at days 1, 6, and 20 was subjected to acRIP-seq, and thus 6 total samples which contained SYN RNA purified from 60 adult mice were sequenced to reveal the ac4C mRNA regulated by learning and memory in the SYN. Two libraries (acRIP and input) were sequenced for each biological sample (Table S3).

The transcripts and ac4C mRNAs identified from the SYN of control mice at days 1, 6 and 20 were largely overlapped (Figure S3A and S3B). Moreover, the low-input acRIP-seq revealed the same consensus motif AGCAGCTG in the ac4C peak regions of SYN mRNA from control mice at days 1, 6 and 20 (Figure S3C). In line with the results from HOM, most ac4C peaks were identified in CDS of SYN mRNA from both control and learning mice (Figure S3D and S3E). These results indicate the consistency of the low-input acRIP-seq for SYN mRNA.

Dynamic change of ac4C mRNA in the SYN of mouse hippocampus during learning and memory

The cumulative distribution of FE of ac4C mRNA in the SYN did not differ between control and learning mice at day 1 (Figure 2F). In contrast, the cumulative distribution curve of FE of ac4C mRNA in the SYN of learning mice had a significant rightward

shift at day 6, compared with that of control mice (Figure 2G). Intriguingly, the cumulative distribution of FE of ac4C mRNA in the SYN of learning mice became indistinguishable from that of control mice at day 20 (Figure 2H). The cumulative distribution of mRNA counts in the SYN remained similar between control and learning mice at days 1, 6, and 20 (Figure 2I-K). These results demonstrate that acetylation of mRNA rather than the total levels of mRNA was increased in the SYN after memory formation but returned to control levels after memory forgetting, further supporting the dynamic change of acetylation of polyA RNA in the SYN during learning and memory (Figure 2B-E).

To identify the learning-induced synaptic ac4C (LISA) mRNA, we analyzed the fold change (FC) of ac4C mRNA in the SYN of learning mice versus control mice (L/C) at days 1, 6, 20 (Figure S3F to S3H). Here we analyzed the average FE of all ac4C peaks to reflect the acetylation level of individual LISA mRNA. Ideally, acetylation of LISA mRNA should be upregulated after memory formation and return to control levels after memory forgetting. In other words, the ac4C of LISA mRNA is specifically upregulated at day 6 (the cut off value of upregulation is FC > 2) but not at days 1 or 20. Per these criteria, we identified 1237 LISA mRNAs whose ac4C levels were increased at day 6 rather than at days 1 or 20 (Figure S3I and Table S4). In contrast, the mRNA levels of LISA were similar at days 1, 6, and 20 (Figure S3I). Gene ontology (GO) analysis indicated that LISA mRNA were significantly enriched in the biological processes (BP) related with synaptic plasticity and learning or memory (Figure 3A and Table S4).

A representative LISA mRNA for Arc

Protein-protein interaction (PPI) network analysis of LISA mRNA involved in the BP of learning or memory revealed several core genes such as Arc, presenilin 1 (Psen1), and Bdnf (Figure 3B). Arc mRNA encodes activity-regulated cytoskeleton associated protein (ARC) and is unique among immediately-early genes (IEG). Arc mRNA can be transported into dendrites and translated near activated postsynaptic sites after neural activities (Lyford et al., 1995; Steward et al., 1998). Different from the regular IEG, Arc

underwent repetitive cycles of transcription and local translation, which is critical for memory consolidation (Das et al., 2023). Although Arc is a promising "master regulator" of protein synthesis-dependent forms of learning and memory, the mechanisms underlying the regulation of local translation of Arc in the SYN remained to be elucidated (Bramham et al., 2010). Analysis of the acRIP-seq data indicate that learning mice have elevated ac4C of Arc mRNA in the SYN at day 6 rather than days 1 or 20, and similar levels of ac4C Arc mRNA in the HOM at day 6, compared with control mice (Figure 3C). The genome browser tracks for the ac4C of all LISA mRNA were accessible at the ac4C website (http://ac4catlas.com/) to show altered ac4C in the SYN, and similar lack of change for those same RNAs in the HOM at day 6.

Next, we used an orthogonal method to verify the dynamic change of ac4C Arc mRNA in the SYN during learning and memory. To this end, performed RT-qPCR analysis for Arc mRNA from the input and acRIP samples purified from the SYN. The levels of input and acRIP-Arc mRNA were similar in the SYN of control and learning mice at days 1 and 20 (Figure 3D, 3E, 3G and 3H). Likewise, the protein levels of ARC were also comparable in the SYN of control and learning mice at days 1 and 20 (Figure 3F and 3I). Although the levels of input Arc mRNA were not altered in the SYN of learning mice at day 6 (Figure 3J), the levels of acRIP-Arc mRNA and ARC proteins were significantly increased in the SYN of learning mice at day 6, compared with controls (Figure 3K and 3L). In contrast, the levels of Arc mRNA and ARC proteins were similar in the HOM of control and learning mice at day 6 (Figure 3M and 3N). Note that Arc mRNA levels in the IgG-IP samples were much lower than that in the acRIP samples (Figure 3E, 3H and 3K), indicating the specificity of RT-qPCR for acRIP. Altogether the results from acRIP-seq and acRIP-qPCR demonstrate that acetylation of Arc mRNA is specifically increased in the SYN after memory formation but returned to control levels after memory forgetting.

Expression of Nat10 in the mature neurons of mouse hippocampus

Since the commercially available NAT10 antibodies were not suitable for immunostaining in the hippocampal slices, we took use of the strategy of genetic

262 labeling (Madisen et al., 2010; Yu et al., 2019) to investigate the expression pattern of
263 Nat10. To this end, a heterozygous knockin mouse line ($Nat10^{Cre/+}$) that expressed the
264 Cre recombinase right after the start codon (ATG) of Nat10 gene was generated using
265 the CRISPR/Cas9 techniques (see details in the Method). Since the Cre recombinase
266 and Nat10 share the same regulatory elements for gene expression in the $Nat10^{Cre/+}$ mice,
267 the Nat10 expression pattern can be revealed through the Cre-reporting adeno-
268 associated virus (AAV) that express EGFP in a Cre-dependent manner. In this way, the
269 Nat10-positive cells would express EGFP in the Nat10 reporter mice (Figure S4A).

270 The dorsal hippocampus integrates multiple synaptic inputs from other brain
271 regions, and is critical for learning and memory (Biane et al., 2023; Fanselow and Dong,
272 2010; Moser et al., 1993). To study the expression pattern of Nat10 in the dorsal
273 hippocampus of adult mice, we injected Cre-reporting AAV into the dorsal
274 hippocampus of 7-week-old $Nat10^{Cre/+}$ mice, and the fluorescent protein EGFP was
275 analyzed 3 weeks after AAV injection. Analysis of the EGFP-positive cells revealed
276 that Nat10 was mainly expressed in the pyramidal cell layer (sp) of CA1 region and
277 granule cell layer (gcl) of dentate gyrus (DG) (Figure S4B). Around 80% of Nat10-
278 expressing cells are mature neurons, evidenced by the overlay between EGFP and NeuN,
279 a protein marker for mature neurons (Figure S4C and S4D). Note that about 20% Nat10-
280 positive cells are non-neuronal cells and probably glia cells. Moreover, about 75% of
281 Nat10-positive cells are excitatory pyramidal neurons in the CA1 region of mouse
282 hippocampus, indicated by the co-localization of EGFP with Neurogranin (NG), a
283 protein marker for excitatory pyramidal neurons (Figure S4C and S4E). These results
284 indicate that Nat10 is mainly expressed by mature neurons in adult mouse hippocampus.

285 To verify that the expression of Cre-reporting AAV has no infection preference
286 toward neurons, we injected the AAV into the dorsal hippocampus of 7-week-old
287 $ALDH1L1^{Cre/ERT2}$ mice, a tamoxifen-induced transgenic Cre line for selectively
288 targeting astrocytes (Srinivasan et al., 2016). After AAV injection for 3 week and
289 tamoxifen gavage for 1 week, we analyzed the expression of the fluorescent protein
290 EGFP in the astrocyte reporter mice (Figure S4F). In the CA1 region of astrocyte

291 reporter mice, EGFP was not expressed in neurons and all EGFP-positive cells show
292 astrocyte-like morphology (Figure S4G). Collectively these results verify the notion
293 that the expression of Cre-reporting AAV has no neuronal preference and strictly
294 depends on the expression pattern of Cre.

295 **Increase of NAT10 proteins in the SYN after learning and memory**

296 The above-mentioned data showed that the levels of ac4C mRNA were increased in the
297 SYN of mouse hippocampus after learning and memory. Next, we aim to investigate
298 whether the protein levels of NAT10, the only known ac4C writer (Liu et al., 2023a),
299 are also regulated by learning and memory. Toward this aim, we purified the SYN
300 fraction from the hippocampus of control and learning mice at days 1, 6 and 20, and
301 analyzed the protein levels of NAT10 by western blots (Figure 4A). The protein levels
302 of NAT10 in the SYN were similar between control and learning mice at day 1 (Figure
303 4B). Interestingly, the protein levels of NAT10 were significantly increased in the SYN
304 of learning mice at day 6, compared with controls (Figure 4C), but returned to control
305 levels at day 20 (Figure 4D). These results indicate that protein levels of NAT10 are
306 increased in the SYN after memory formation but return to normal levels after memory
307 forgetting (Figure 4E).

308 The increase of NAT10 proteins in the SYN at day 6 could be due to the
309 upregulation of NAT10 in the HOM (i.e., the increase of de novo protein synthesis).
310 However, the protein levels of NAT10 were not altered in HOM of learning mice at day
311 6, compared to controls (Figure 4F), suggesting that learning and memory did not
312 upregulate the de novo protein synthesis of NAT10 in mouse hippocampus. To further
313 explore the distribution of NAT10 proteins in other subcellular fractions, we purified
314 the nucleus (N), cytoplasm (S2) and post-synaptic density (PSD) fractions from the
315 hippocampus of control and learning mice at day 6, and analyzed the protein levels of
316 NAT10 in different subcellular fractions (Figure 4G). The nuclear fraction was enriched
317 for histone but was depleted of cytoplasmic protein α-tubulin or synaptic protein SYN1
318 and PSD95, and vice versa for the S2 and PSD fraction (Figure 4H). The protein levels
319 of NAT10 in the nucleus did not change at day 6 after learning and memory (Figure 4I).

320 Strikingly, the NAT10 proteins were significantly reduced in the cytoplasm (S2 fraction)
321 but increased in the PSD fraction at day 6 after learning and memory (Figure 4J and
322 4K). These results suggest that NAT10 proteins might be relocated from the cytoplasm
323 to synapses in mouse hippocampus after memory formation.

324 NAT10 belongs to the p300/CBP-associated factor (PCAF) subfamily of protein
325 acetyltransferase (Lau et al., 2000). Next, we aim to investigate whether learning and
326 memory also changed protein levels of PCAF in the subcellular fractions of mouse
327 hippocampus. The protein levels of PCAF did not change in the nucleus, cytoplasm or
328 PSD fractions of learning mice at day 6, compared with controls (Figure 4L-N),
329 indicating that learning and memory may not alter the subcellular distribution of PCAF.

330 Next, we performed immunofluorescent staining to study the synaptic distribution
331 of NAT10 proteins before and after chemical LTP stimulation in cultured hippocampal
332 neurons (Figure S5A) – a cellular model of learning and memory (Lu et al., 2001; Shahi
333 and Baudry, 1993). In control neurons treated with vehicle, NAT10 was mainly
334 expressed in the nucleus and cytoplasm (Figure S5B), which is consistent with the
335 results of western blots (Figure 4I and 4J). However, 60 minutes after chemical LTP
336 stimulation, the colocalization of NAT10 with PSD95, a protein marker for PSD
337 fraction, was significantly increased, compared with control neurons (Figure S5C and
338 S5D). These results indicated that distribution of NAT10 in the PSD were increased in
339 cultured hippocampal neurons after chemical LTP stimulation, which support the
340 increased protein levels of NAT10 in the PSD fraction of mouse hippocampus after
341 learning and memory (Figure 4K).

342 **NAT10-dependent ac4C modification of polyA RNA in mouse hippocampus**

343 To demonstrate the NAT10-dependent ac4C modification of poly A RNA, we used the
344 Cre/Loxp strategy (Tsien et al., 1996) to downregulate Nat10 expression in adult mouse
345 hippocampus through injection of AAV-EGFP (as a control) or AAV-EGFP-P2A-Cre
346 into the hippocampus of $Nat10^{flox/flox}$ mice. Given that Nat10 is mainly expressed in the
347 mature neurons (Figure S4), the expression of EGFP or EGFP-2A-Cre in the AAV was
348 driven by the human synapsin 1 (Syn1) promoter, a neuron-specific promoter

349 (Hedegaard et al., 2013). The Nat10$^{flox/flox}$ mice injected with AAV-EGFP and AAV-
350 EGFP-P2A-Cre were named control and Nat10 conditional knockout (cKO) mice
351 hereafter. Both the control and Nat10 cKO mice received stereotaxic AAV injection into
352 the dorsal hippocampus, and the HOM of dorsal hippocampus were collected for
353 biochemical assay 3 weeks after AAV injection (Figure S6A).

354 The fluorescent protein EGFP was expressed mainly in the CA1-3 regions and DG
355 of mouse hippocampus 3 weeks after AAV injection (Figure S6B), indicating the
356 successful infection of AAV. The protein levels of NAT10 were significantly reduced in
357 the hippocampus of Nat10 cKO mice, compared with controls (Figure S6C and S6D),
358 thereby verifying the effective knockdown of NAT10 by the Cre/Loxp strategy. NAT10
359 was previously described as a protein acetyltransferase against α-tubulin and histones
360 (Lv et al., 2003; Shen et al., 2009). However, immunoblotting with acetylation-specific
361 antibodies showed no significant change of protein acetylation in Nat10 cKO
362 hippocampus, compared to controls (Figure S6C, S6E and S6F). These results suggest
363 the redundancy of acetyltransferases for α-tubulin and histones in mouse hippocampus.
364 In contrast, the ac4C modification of polyA RNA was significantly decreased in the
365 Nat10 cKO mice, compared with controls (Figure S6G and S6H). As a control
366 experiment, downregulation of NAT10 did not affect the m6A modification of polyA
367 RNA (Figure S6I and S6J). The LC-MS/MS analysis of polyA RNA indicated that the
368 stoichiometry levels of ac4C rather than m6A were significantly reduced in the
369 hippocampus of Nat10 cKO mice, compared with controls (Figure S6K and S6L).
370 Altogether these results demonstrate that NAT10 specifically regulates ac4C rather than
371 m6A of polyA RNA in mouse hippocampus.

372 **NAT10-dependent ac4C mapping of SYN mRNAs in learning mice**

373 Given that learning and memory increased ac4C mRNA specifically in the SYN, we
374 next aim to identify NAT10-dependent ac4C modification of synaptic mRNA. To this
375 end, we performed low-input acRIP-seq for SYN RNA purified from the hippocampus
376 of control and Nat10 cKO mice at day 6 after learning and memory (Figure 5A). Due
377 to the limited yield of SYN RNA, we purified SYN RNA from the hippocampus of 10

mice and combined them into one sample. Two biological samples from the respective control and Nat10 cKO mice at day 6 were subjected to low-input acRIP-seq to demonstrate the NAT10-dependent ac4C modification of SYN mRNA. Two libraries (acRIP and input) were sequenced for each biological sample (Table S3).

We identified 7097 and 1933 ac4C peaks from the SYN of control and Nat10 cKO mice, respectively (Figure 5B). These results suggest a reduction of the a4C peak number by conditional knockout of Nat10 in mature neurons of adult mouse hippocampus. Out of 7097 ac4C peaks identified in control mice, 6331 peaks were abolished and 408 peaks were downregulated in Nat10 cKO mice, and these ac4C peaks (total 6739) were named NAT10-dependent ac4C peaks (Figure 5C) which were mainly localized in the CDS region of mRNA (Figure 5D).

The Nat10 cKO mice also showed a reduction of ac4C mRNA number identified in the SYN, compared with controls (Figure 5E). In contrast, the number of mRNA identified in the SYN was similar between control and Nat10 cKO mice (Figure 5F). Likewise, the total levels of ac4C mRNA were significantly reduced in the SYN of Nat10 cKO mice, compared with controls, as evidenced by the leftward-shifted cumulative distribution curve of FE of ac4C mRNA in the Nat10 cKO mice (Figure 5G). In contrast, the cumulative distribution curve of mRNA counts were similar in the SYN of control and Nat10 cKO mice (Figure 5H). Out of 3778 ac4C mRNAs identified in the SYN of control mice, 2507 ac4C mRNAs were diminished and 839 ac4C mRNAs were downregulated in the Nat10 cKO mice, and these ac4C mRNAs (total 3346) were named NAT10-dependent synaptic ac4C (NASA) mRNA (Figure 5I and Table S5).

We next analyzed the cellular expression pattern of NASA mRNA through the single-cell RNA-seq atlas of mouse hippocampus (dropviz.org) (Saunders et al., 2018). The results indicated that the expression of NASA mRNA was mostly enriched in excitatory neurons (Figure 5J), which is in line with the cellular expression pattern of NAT10 in mouse hippocampus (Figure S4). In addition, about 13% of NASA mRNAs were relatively enriched in glia cells (Figure 5J), which is consistent with the notion that processes of glia cells contribute to formation of the tripartite synapses (Eroglu and

407 Barres, 2010; Perea et al., 2009). Gene ontology (GO) analysis showed that NASA
408 mRNAs were significantly enriched in the biological processes (BP) related with
409 synaptic plasticity and learning or memory (Figure 5K and Table S5).

410 **Regulation of ac4C and protein levels of Arc, Camk2α and Grin2b in the SYN by**
411 **NAT10**

412 Twenty-seven NASA mRNAs implicated in the BP of synaptic plasticity and learning
413 or memory also belong to LISA mRNA (Figure 6A and Table S4), which we named
414 class 1 mRNA. In contrast, 212 NASA mRNAs related with synaptic plasticity and
415 learning or memory did not belong to LISA mRNA (Figure 6A and Table S5), which
416 we named class 2 mRNA. Analysis of the protein-protein interaction (PPI) network
417 revealed significant interaction between the mRNAs in both class 1 and class 2.
418 Remarkably, 14 out of the 27 mRNAs in class 1 were found to be interconnected (Figure
419 6B), and 199 out of the 212 mRNAs in class 2 formed a PPI network (Figure 6C).

420 Arc, a representative LISA mRNA (Figure 3), was found in the PPI network of
421 class 1 mRNA. The mRNA of Ca^{2+}/calmodulin-dependent protein kinase 2α (Camk2α)
422 and Grin 2b encode the protein kinase CaMK2α and the GluN2B subunit of NMDA
423 receptor, respectively. CaMK2α and GluN2B are synapse-enriched proteins and play
424 important roles in LTP as well as learning and memory (Lisman et al., 2012; Tang et al.,
425 1999). Recent studies demonstrate that CaMK2α interaction with GluN2B is critical
426 for the induction and maintenance of LTP (Chen et al., 2024; Tullis et al., 2023). Both
427 Camk2α and Grin 2b were identified in the PPI network of class 2 mRNA. Analysis of
428 the low-input acRIP-seq data indicated the reduction of ac4C peaks of Arc,
429 Camk2α and Grin 2b mRNA in the SYN of Nat10 cKO mice, compared with controls
430 (Figure 6D-F). The genome browser tracks for the ac4C of all NASA mRNAs were
431 accessible at the ac4C website (http://ac4catlas.com/) to show reduced or diminished
432 ac4C peaks in the SYN of Nat10 cKO mice, compared with controls.

433 Next, we performed RT-qPCR analysis for input and acRIP RNAs purified from
434 the SYN of control and Nat10 cKO mice at day 6 after learning and memory to verify
435 the NAT10-dependent ac4C modification of Arc, Camk2α and Grin2b mRNA (Figure

436 6G). As shown in Figure 6H, the input mRNA levels of Arc, Camk2α and Grin2b in the
437 SYN were comparable between control and Nat10 cKO mice. In contrast, the acRIP
438 mRNA levels of Arc, Camk2α and Grin2b in the SYN were significantly reduced in
439 Nat10 cKO mice, compared with controls (Figure 6I). Given that ac4C modification of
440 mRNA has been shown to enhance translation efficiency (Arango et al., 2018; Arango
441 et al., 2022), we sought to determine whether Nat10 influences the protein levels of
442 ARC, CaMK2α and GluN2B in the SYN by western blot analysis (Figure 6G). The
443 protein levels of ARC, CaMK2α and GluN2B were significantly decreased in the SYN
444 at day 6 from Nat10 cKO mice, compared with controls (Figure 6J). Altogether, these
445 results demonstrate that Nat10 regulates ac4C and protein levels, rather than mRNA
446 levels of Arc, Camk2α and Grin2b in the SYN of mouse hippocampus at day 6 in the
447 MWM.

448 **Regulation of LTP as well as learning and memory by NAT10 in mouse**
449 **hippocampus**

450 In the following study, we investigate whether Nat10 in mouse hippocampus is
451 important for LTP as well as learning and memory. The body and brain weight were
452 similar between control and Nat10 cKO mice (Figure S7A and S7B). The number and
453 intrinsic excitability of CA1 pyramidal neurons were also comparable between control
454 and Nat10 cKO mice (Figure S7C and S7D). To address whether Nat10 regulates LTP,
455 we performed electrophysiology recording of fEPSP (field excitatory postsynaptic
456 potential) at the SC-CA1 synapses before and after high frequency stimulation (HFS)
457 (Figure 7A). The induction of LTP was comparable between control and Nat10 cKO
458 mice (Figure 7B-D). However, the maintenance of LTP especially the late phase of LTP
459 was severely impaired in Nat10 cKO mice, compared with controls (Figure 7B, 7C, 7E
460 and 7F).

461 To further study whether Nat10 is important for synaptic plasticity after learning
462 and memory, we performed fEPSP recording to investigate glutamatergic transmission
463 at the SC-CA1 synapses in the control and Nat10 cKO mice at day 6 after learning and
464 memory (Figure 7G). Consistent with the previous report (Su et al., 2023), the

465 glutamatergic transmission at the SC-CA1 synapses was significantly enhanced at day
466 6 in learning mice, compared with mice without learning (Figure 7H and 7I). The
467 glutamatergic transmission at the SC-CA1 synapses was similar between control and
468 Nat10 cKO mice without learning, which indicate that Nat10 may be dispensable for
469 the glutamatergic transmission at the SC-CA1 synapses at basal conditions. However,
470 the learning and memory-induced enhancement of glutamatergic transmission at the
471 SC-CA1 synapses was significantly impaired in Nat10 cKO mice, compared with
472 controls (Figure 7H and 7I). Altogether these results indicate that NAT10 is important
473 for synaptic plasticity related with learning and memory in mouse hippocampus.

474 To investigate whether NAT10 is critical for learning and memory, both control and
475 Nat10 cKO mice were subjected to training in the MWM for 5 days, and the probe test
476 was performed at day 6 (Figure 7G). Both groups exhibited an overall decline in the
477 latency to reach the platform at the early stage (day 1-2) of training (Figure 7J).
478 However, the Nat10 cKO mice failed to improve performance during the late training
479 stage (day 3-5), compared with controls (Figure 7J). During the probe tests, the control
480 and Nat10 cKO mice showed similar distance travelled (Figure 7K and 7L). However,
481 the time spent in the target area and the number of platform crossing were significantly
482 reduced during the probe test in Nat10 cKO mice, compared with controls (Figure 7L-
483 N). These results demonstrate that NAT10 in mouse hippocampus is important for
484 spatial learning and memory.

485

486 **Discussion**

487 In this study, we demonstrate the dynamic regulation of synaptic mRNA acetylation by
488 learning and memory in mouse hippocampus. We identified ~1200 ac4C-modified
489 mRNAs (i.e., LISA mRNA) that were increased in the SYN of mouse hippocampus
490 after memory formation but returned to normal levels after memories were naturally
491 forgotten. In contrast, LISA mRNAs were not increased in the HOM of mouse
492 hippocampus after learning and memory. Interestingly, the protein levels of NAT10
493 were also increased in the SYN after memory formation but returned to control levels

after forgetting. We further showed NAT10-dependent ac4C mapping of SYN mRNAs through the acRIP-seq from control and Nat10 cKO mice. In addition, we performed RT-qPCR analysis of acRIP and input RNA to verify the NAT10-dependent ac4C modification of synaptic Arc, Camk2α and Grin2b mRNAs. Genetic ablation of NAT10 in adult mouse hippocampus also reduced the protein rather than mRNA levels of Arc and Camk2α and Grin2b in the SYN at day 6 in the MWM. Lastly, the maintenance of LTP at the SC-CA1 synapses as well as the behaviors of learning and memory were severely impaired in the Nat10 cKO mice. In sum, these results demonstrate the potential contribution of NAT10-mediated ac4C modification of mRNA to synaptic plasticity and memory.

The dynamic regulation of protein acetylation in the SYN by learning and memory has been shown in our previous studies (Zhang et al., 2021a; Zhang et al., 2021b; Zhang et al., 2021c; Zhang et al., 2024). In contrast to the well-characterized acetyltransferases and deacetylases for protein acetylation (Drazic et al., 2016), the writer and eraser of mRNA acetylation are less well understood. The NAT10 acetyltransferase is the only known ac4C writer in the mammalian cells (Cui et al., 2023; Hu *et al.*, 2024a). Recently, the deacetylase SIRT7 has been shown to erase the ac4C modification of ribosomal RNA (rRNA) and small nucleolar RNA (snoRNA) (Kudrin et al., 2021; Xu et al., 2021). However, the mechanisms underlying the deacetylation of mRNA needs further exploration.

How the ac4C modification of mRNA is regulated by neural activities remains largely unknown. Our previous studies showed that overnight starvation downregulated the ac4C modification of tyrosine hydroxylase (TH) mRNA in the sympathetic nerve terminus that innervate the olfactory mucosa in mice, which reduced TH protein levels and dopamine synthesis in the mouse olfactory mucosa after overnight starvation (Zhou et al., 2022). In this study, we demonstrate that learning and memory regulate the dynamic change of ac4C modification of mRNA at synapses of mouse hippocampus. Altogether these studies provide evidence that neural activities regulate acetylation of mRNA in a spatiotemporally specific manner.

523 NAT10 proteins were increased in the SYN but reduced in the cytoplasm of mouse
524 hippocampus at day 6 in the MWM. These results suggest a relocation of NAT10 from
525 the cytoplasm to synapses after learning and memory, which was corroborated by the
526 immunostaining study of NAT10 distribution in cultured mouse hippocampal neurons
527 after cLTP stimulation. Previous proteomic studies showed that NAT10 were detected
528 in the interactome with several motor proteins such as kinesin proteins (Rouillard et al.,
529 2016), which raised the possibility that NAT10 might be transported by the motor
530 proteins in hippocampal neurons during learning and memory. NAT10 was highly
531 expressed in the nucleus of hippocampal neurons, but protein levels of nuclear NAT10
532 were not altered at day 6 in the MWM. NAT10 has been shown to be important for
533 regulating nuclear functions such as nucleolar assembly (Shen et al., 2009) and nuclear
534 architecture (Larrieu et al., 2014). The function of NAT10 in the nucleus of neurons
535 waits for future investigations.

536 The subcellular change of NAT10 proteins at day 6 apparently may not be caused
537 by stress during the training in the MWM. The mice were well handled before and
538 during the training, and thus the stress should be minor if any. The control mice were
539 exposed to the training using visible platform at day 1, the stress levels in the control
540 mice may be vary with the learning mice. If mild stress during the training in the MWM
541 could cause the relocation of NAT10 to the SYN, the protein levels of NAT10 in the
542 SYN would be increased at day 1. However, the protein levels of NAT10 in the SYN
543 were similar at day 1 between control and learning mice. In addition, chronic mild stress
544 has been shown to increase the total protein levels of NAT10 in mouse hippocampus
545 (Guo et al., 2022). In contrast, the total protein levels of NAT10 in mouse hippocampus
546 did not alter at day 6 in the MWM. These results suggest that the increased NAT10
547 proteins in the SYN at day 6 in the MWM may be related with learning and memory
548 rather than stress.

549 The stoichiometry levels of ac4C in polyA RNA has been reported to be ~0.2% in
550 HeLa cells (Arango *et al.*, 2018), ~0.1% in human embryonic stem cells (Hu et al.,
551 2024b), ~0.2% in liver (Hao et al., 2022), and ~0.3% in heart (Shi et al., 2023b). Here

we showed that ~0.4% of cytidine was acetylated in mouse hippocampus. Although the total protein levels of NAT10 has been reported to be relatively lower in the whole brain tissue compared with other tissues (Jiang *et al.*, 2023), the NAT10 was shown to be highly expressed in hippocampal neurons (Gao et al., 2024). Future studies are warranted to investigate how the acetyltransferase activity of NAT10 toward mRNA was regulated in different brain regions and different tissues.

The basal glutamatergic transmission at the SC-CA1 synapses were unaltered in the Arc knockout mice (Plath et al., 2006), which is consistent with the phenotypes in the Nat10 cKO mice. On the other hand, ARC has been shown to accelerate AMPA receptor endocytosis (Chowdhury et al., 2006), and thus the induction of LTP at the SC-CA1 synapses was enhanced in the Arc knockout mice (Plath *et al.*, 2006). Although ARC protein levels were decreased in the SYN of Nat10 cKO mice, the induction of LTP at the SC-CA1 synapses was not increased in the Nat10 cKO mice. These results might be due to the reduction of other LTP-promoting proteins such as CaMK2α and GluN2b in the SYN of Nat10 cKO mice.

In line with the phenotypes of Nat10 cKO mice presented in this study, the Arc knockout mice showed deficits in the late phase of LTP at SC-CA1 synapses and impairment of memory consolidation in the MWM (Plath *et al.*, 2006). Consistent with the function of Arc in memory consolidation, the acetylation of Arc mRNA was increased in the SYN at day 6 rather than day 1 following MWM training, a period during which memories were consolidated. Moreover, the increase of ac4C and protein levels of Arc in the SYN at day 6 was NAT10-dependent, which might underlie the contribution of NAT10 in learning and memory. However, the function of NAT10 in regulating tRNA or rRNA might also contribute to learning and memory. New techniques for overexpression and erasure of site-specifically acetylated mRNA need to be developed to precisely study the function of mRNA acetylation. Nonetheless, the results presented here demonstrate the dynamic regulation and potential importance of synaptic mRNA acetylation in learning and memory.

References

Arango, D., Sturgill, D., Alhusaini, N., Dillman, A.A., Sweet, T.J., Hanson, G., Hosogane, M., Sinclair, W.R., Nanan, K.K., and Mandler, M.D. (2018). Acetylation of cytidine in mRNA promotes translation efficiency. Cell *175*, 1872-1886.

Arango, D., Sturgill, D., Yang, R., Kanai, T., Bauer, P., Roy, J., Wang, Z., Hosogane, M., Schiffers, S., and Oberdoerffer, S. (2022). Direct epitranscriptomic regulation of mammalian translation initiation through N4-acetylcytidine. *Mol Cell 82*, 2797-2814.

Beiki, H., Sturgill, D., Arango, D., Relier, S., Schiffers, S., and Oberdoerffer, S. (2024). Detection of ac4C in human mRNA is preserved upon data reassessment. *Mol Cell 84*, 1611-1625. e1613.

Besse, F., and Ephrussi, A. (2008). Translational control of localized mRNAs: restricting protein synthesis in space and time. *Nat Rev Mol Cell Biol 9*, 971-980.

Biane, J.S., Ladow, M.A., Stefanini, F., Boddu, S.P., Fan, A., Hassan, S., Dundar, N., Apodaca-Montano, D.L., Zhou, L.Z., and Fayner, V. (2023). Neural dynamics underlying associative learning in the dorsal and ventral hippocampus. *Nat Neurosci 26*, 798-809.

Biever, A., Glock, C., Tushev, G., Ciirdaeva, E., Dalmay, T., Langer, J.D., and Schuman, E.M. (2020). Monosomes actively translate synaptic mRNAs in neuronal processes. *Science 367*, eaay4991.

Bliss, T.V., and Collingridge, G.L. (1993). A synaptic model of memory: long-term potentiation in the hippocampus. *Nature 361*, 31-39.

Boccaletto, P., Machnicka, M.A., Purta, E., Piątkowski, P., Bagiński, B., Wirecki, T.K., de Crécy-Lagard, V., Ross, R., Limbach, P.A., and Kotter, A. (2018). MODOMICS: a database of RNA modification pathways. 2017 update. *Nucleic Acids Res 46*, D303-D307.

Bramham, C.R., Alme, M.N., Bittins, M., Kuipers, S.D., Nair, R.R., Pai, B., Panja, D., Schubert, M., Soule, J., Tiron, A., and Wibrand, K. (2010). The Arc of synaptic memory. *Exp Brain Res 200*, 125-140.

Cajigas, I.J., Tushev, G., Will, T.J., tom Dieck, S., Fuerst, N., and Schuman, E.M. (2012). The local transcriptome in the synaptic neuropil revealed by deep sequencing and high-resolution imaging. *Neuron 74*, 453-466.

Chen, X., Cai, Q., Zhou, J., Pleasure, S.J., Schulman, H., Zhang, M., and Nicoll, R.A. (2024). CaMKII autophosphorylation is the only enzymatic event required for synaptic memory. *Proc Natl Acad Sci U S A 121*, e2402783121.

Chowdhury, S., Shepherd, J.D., Okuno, H., Lyford, G., Petralia, R.S., Plath, N., Kuhl, D., Huganir, R.L., and Worley, P.F. (2006). Arc/Arg3.1 interacts with the endocytic machinery to regulate AMPA receptor trafficking. *Neuron 52*, 445-459.

Cui, Z., Xu, Y., Wu, P., Lu, Y., Tao, Y., Zhou, C., Cui, R., Li, J., and Han, R. (2023). NAT10 promotes osteogenic differentiation of periodontal ligament stem cells by regulating VEGFA-mediated PI3K/AKT signaling pathway through ac4C modification. *Odontology 111*, 870-882.

Das, S., Lituma, P.J., Castillo, P.E., and Singer, R.H. (2023). Maintenance of a short-lived protein required for long-term memory involves cycles of transcription and local translation. *Neuron 111*, 2051-2064

Day, J.J., and Sweatt, J.D. (2011). Epigenetic mechanisms in cognition. *Neuron 70*, 813-829.
Drazic, A., Myklebust, L.M., Ree, R., and Arnesen, T. (2016). The world of protein acetylation.
Biochim Biophys Acta 1864, 1372-1401.
Eroglu, C., and Barres, B.A. (2010). Regulation of synaptic connectivity by glia. *Nature 468*, 223-231.
Fanselow, M.S., and Dong, H.-W. (2010). Are the dorsal and ventral hippocampus functionally distinct structures? *Neuron 65*, 7-19.
Fischer, A., Sananbenesi, F., Wang, X., Dobbin, M., and Tsai, L.-H. (2007). Recovery of learning and memory is associated with chromatin remodelling. *Nature 447*, 178-182.
Gao, S., Shen, R., Li, J., Jiang, Y., Sun, H., Wu, X., Li, X., Miao, C., He, M., Wang, J., and Chen, W. (2024). N-acetyltransferase 10 mediates cognitive dysfunction through the acetylation of GABABR1 mRNA in sepsis-associated encephalopathy. *Proc Natl Acad Sci U S A 121*, e2410564121.
Georgeson, J., and Schwartz, S. (2024). No evidence for ac4C within human mRNA upon data reassessment. *Mol Cell 84*, 1601-1610.
Goldie, B.J., and Cairns, M.J. (2012). Post-transcriptional trafficking and regulation of neuronal gene expression. *Mol Neurobiol 45*, 99-108.
Guca, E., Alarcon, R., Palo, M.Z., Santos, L., Alonso-Gil, S., Davyt, M., de Lima, L.H., Boissier, F., Das, S., and Zagrovic, B. (2024). N6-methyladenosine in 5′ UTR does not promote translation initiation. *Mol Neurobiol 84*, 584-595.
Guo, X.-F., Wang, X.-H., Fu, Y.-L., Meng, Q., Huang, B.-Y., Yang, R., Guo, Y., Du, Y.-R., Wang, X., and Gao, Y. (2022). Elevation of N-acetyltransferase 10 in hippocampal neurons mediates depression-and anxiety-like behaviors. *Brain Res Bull 185*, 91-98.
Hafner, A.S., Donlin Asp, P.G., Leitch, B., Herzog, E., and Schuman, E.M. (2019). Local protein synthesis is a ubiquitous feature of neuronal pre-and postsynaptic compartments. *Science 364*, eaau3644.
Hao, H., Liu, W., Miao, Y., Ma, L., Yu, B., Liu, L., Yang, C., Zhang, K., Chen, Z., Yang, J., et al. (2022). N4-acetylcytidine regulates the replication and pathogenicity of enterovirus 71. *Nucleic Acids Res 50*, 9339-9354.
Hedegaard, C., Kjaer-Sorensen, K., Madsen, L.B., Henriksen, C., Momeni, J., Bendixen, C., Oxvig, C., and Larsen, K. (2013). Porcine synapsin 1: SYN1 gene analysis and functional characterization of the promoter. *FEBS Open Bio 3*, 411-420.
Heinz, S., Benner, C., Spann, N., Bertolino, E., Lin, Y.C., Laslo, P., Cheng, J.X., Murre, C., Singh, H., and Glass, C.K. (2010). Simple combinations of lineage-determining transcription factors prime cis-regulatory elements required for macrophage and B cell identities. *Mol Cell 38*, 576-589.
Hoz, L.d., Martin, S.J., and Morris, R.G.M. (2004). Forgetting, reminding, and remembering: the retrieval of lost spatial memory. *PLoS Biol 2*, e225.
Hu, Z., Lu, Y., Cao, J., Lin, L., Chen, X., Zhou, Z., Pu, J., Chen, G., Ma, X., and Deng, Q. (2024a). N-acetyltransferase NAT10 controls cell fates via connecting mRNA cytidine acetylation to chromatin signaling. *Sci Adv 10*, eadh9871.

669 Ito, S., Akamatsu, Y., Noma, A., Kimura, S., Miyauchi, K., Ikeuchi, Y., Suzuki, T., and
670 Suzuki, T. (2014a). A single acetylation of 18 S rRNA is essential for biogenesis of the
671 small ribosomal subunit in Saccharomyces cerevisiae. *J Biol Chem 289*, 26201-26212.
672 Ito, S., Horikawa, S., Suzuki, T., Kawauchi, H., Tanaka, Y., Suzuki, T., and Suzuki, T.
673 (2014b). Human NAT10 is an ATP-dependent RNA acetyltransferase responsible for
674 N4-acetylcytidine formation in 18 S ribosomal RNA (rRNA). *J Biol Chem 289*, 35724-
675 35730.
676 Jarrard, L.E. (1993). On the role of the hippocampus in learning and memory in the rat.
677 *Behav Neural Biol 60*, 9-26.
678 Jiang, X., Cheng, Y., Zhu, Y., Xu, C., Li, Q., Xing, X., Li, W., Zou, J., Meng, L., and
679 Azhar, M. (2023). Maternal NAT10 orchestrates oocyte meiotic cell-cycle progression
680 and maturation in mice. *Nat Commun 14*, 3729.
681 Kouzarides, T. (2007). Chromatin modifications and their function. *Cell 128*, 693-705.
682 Kowalski, S., Yamane, T., and Fresco, J.R. (1971). Nucleotide sequence of the
683 "denaturable" leucine transfer RNA from yeast. *Science 172*, 385-387.
684 Kruppa, J., and Zachau, H.G. (1972). Multiplicity of serine-specific transfer RNAs of
685 brewer's and baker's yeast. *Biochim Biophys Acta 277*, 499-512.
686 Kudrin, P., Meierhofer, D., Vågbø, C.B., and Ørom, U.A.V. (2021). Nuclear RNA-
687 acetylation can be erased by the deacetylase SIRT7. BioRxiv, 2021.04.06.438707.
688 Larrieu, D., Britton, S., Demir, M., Rodriguez, R., and Jackson, S.P. (2014). Chemical
689 inhibition of NAT10 corrects defects of laminopathic cells. *Science 344*, 527-532.
690 Lau, O.D., Courtney, A.D., Vassilev, A., Marzilli, L.A., Cotter, R.J., Nakatani, Y., and
691 Cole, P.A. (2000). p300/CBP-associated factor histone acetyltransferase processing of
692 a peptide substrate: kinetic analysis of the catalytic mechanism. *J Biol Chem 275*,
693 21953-21959.
694 Levenson, J.M., O'Riordan, K.J., Brown, K.D., Trinh, M.A., Molfese, D.L., and Sweatt,
695 J.D. (2004). Regulation of histone acetylation during memory formation in the
696 hippocampus. *J Biol Chem 279*, 40545-40559.
697 Levenson, J.M., and Sweatt, J.D. (2005). Epigenetic mechanisms in memory formation.
698 *Nat Rev Neurosci 6*, 108-118.
699 Li, B., Xi, W., Bai, Y., Liu, X., Zhang, Y., Li, L., Bian, L., Liu, C., Tang, Y., Shen, L., et
700 al. (2023). FTO-dependent m(6)A modification of Plpp3 in circSCMH1-regulated
701 vascular repair and functional recovery following stroke. *Nat Commun 14*, 489.
702 Lisman, J., Yasuda, R., and Raghavachari, S. (2012). Mechanisms of CaMKII action in
703 long-term potentiation. *Nat Rev Neurosci 13*, 169-182.
704 Liu, R., Wubulikasimu, Z., Cai, R., Meng, F., Cui, Q., Zhou, Y., and Li, Y. (2023a).
705 NAT10-mediated N4-acetylcytidine mRNA modification regulates self-renewal in
706 human embryonic stem cells. *Nucleic Acids Res 51*, 8514-8531.
707 Liu, Y., Wang, X., Liu, Y., Yang, J., Mao, W., Feng, C., Wu, X., Chen, X., Chen, L., and
708 Dong, P. (2023b). N4-acetylcytidine-dependent GLMP mRNA stabilization by NAT10
709 promotes head and neck squamous cell carcinoma metastasis and remodels tumor
710 microenvironment through MAPK/ERK signaling pathway. *Cell Death Dis 14*, 712.
711 Lu, W., Man, H., Ju, W., Trimble, W.S., MacDonald, J.F., and Wang, Y.T. (2001).
712 Activation of synaptic NMDA receptors induces membrane insertion of new AMPA

receptors and LTP in cultured hippocampal neurons. *Neuron 29*, 243-254.
Lv, J., Liu, H., Wang, Q., Tang, Z., Hou, L., and Zhang, B. (2003). Molecular cloning of a novel human gene encoding histone acetyltransferase-like protein involved in transcriptional activation of hTERT. *Biochem Biophys Res Commun 311*, 506-513.
Lyford, G.L., Yamagata, K., Kaufmann, W.E., Barnes, C.A., Sanders, L.K., Copeland, N.G., Gilbert, D.J., Jenkins, N.A., Lanahan, A.A., and Worley, P.F. (1995). Arc, a growth factor and activity-regulated gene, encodes a novel cytoskeleton-associated protein that is enriched in neuronal dendrites. *Neuron 14*, 433-445.
Madisen, L., Zwingman, T.A., Sunkin, S.M., Oh, S.W., Zariwala, H.A., Gu, H., Ng, L.L., Palmiter, R.D., Hawrylycz, M.J., and Jones, A.R. (2010). A robust and high-throughput Cre reporting and characterization system for the whole mouse brain. *Nat Neurosci 13*, 133-140.
Martin, K.C., Barad, M., and Kandel, E.R. (2000). Local protein synthesis and its role in synapse-specific plasticity. *Curr Opin Neurobiol 10*, 587-592.
Merkurjev, D., Hong, W.-T., Iida, K., Oomoto, I., Goldie, B.J., Yamaguti, H., Ohara, T., Kawaguchi, S.-y., Hirano, T., and Martin, K.C. (2018). Synaptic N 6-methyladenosine (m6A) epitranscriptome reveals functional partitioning of localized transcripts. *Nat Neurosci 21*, 1004-1014.
Morris, R. (1984). Developments of a water-maze procedure for studying spatial learning in the rat. *J Neurosci Methods 11*, 47-60.
Moser, E., Moser, M.-B., and Andersen, P. (1993). Spatial learning impairment parallels the magnitude of dorsal hippocampal lesions, but is hardly present following ventral lesions. *J Neurosci 13*, 3916-3925.
Moser, M.-B., Trommald, M., and Andersen, P. (1994). An increase in dendritic spine density on hippocampal CA1 pyramidal cells following spatial learning in adult rats suggests the formation of new synapses. *Proc Natl Acad Sci U S A 91*, 12673-12675.
Newman, A.M., Liu, C.L., Green, M.R., Gentles, A.J., Feng, W., Xu, Y., Hoang, C.D., Diehn, M., and Alizadeh, A.A. (2015). Robust enumeration of cell subsets from tissue expression profiles. *Nat Methods 12*, 453-457.
Niu, M., Cao, W., Wang, Y., Zhu, Q., Luo, J., Wang, B., Zheng, H., Weitz, D.A., and Zong, C. (2023). Droplet-based transcriptome profiling of individual synapses. *Nat Biotechnol 41*, 1332-1344.
Oashi, Z., Murao, K., Yahagi, T., Von Minden, D.L., McCloskey, J.A., and Nishimura, S. (1972). Characterization of C + located in the first position of the anticodon of Escherichia coli tRNA Met as N 4 -acetylcytidine. *Biochim Biophys Acta 262*, 209-213.
Perea, G., Navarrete, M., and Araque, A. (2009). Tripartite synapses: astrocytes process and control synaptic information. *Trends Neurosci 32*, 421-431.
Plath, N., Ohana, O., Dammermann, B., Errington, M.L., Schmitz, D., Gross, C., Mao, X., Engelsberg, A., Mahlke, C., and Welzl, H. (2006). Arc/Arg3. 1 is essential for the consolidation of synaptic plasticity and memories. *Neuron 52*, 437-444.
Rouillard, A.D., Gundersen, G.W., Fernandez, N.F., Wang, Z., Monteiro, C.D., McDermott, M.G., and Ma'ayan, A. (2016). The harmonizome: a collection of processed datasets gathered to serve and mine knowledge about genes and proteins. *Database (Oxford) 2016, baw100*.

Saunders, A., Macosko, E.Z., Wysoker, A., Goldman, M., Krienen, F.M., de Rivera, H., Bien, E., Baum, M., Bortolin, L., Wang, S., et al. (2018). Molecular Diversity and Specializations among the Cells of the Adult Mouse Brain. *Cell 174*, 1015-1030

Shahi, K., and Baudry, M. (1993). Glycine-induced changes in synaptic efficacy in hippocampal slices involve changes in AMPA receptors. *Brain Res 627*, 261-266.

Shen, Q., Zheng, X., McNutt, M.A., Guang, L., Sun, Y., Wang, J., Gong, Y., Hou, L., and Zhang, B. (2009). NAT10, a nucleolar protein, localizes to the midbody and regulates cytokinesis and acetylation of microtubules. *Exp Cell Res 315*, 1653-1667.

Shi, H., Zhang, X., Weng, Y.-L., Lu, Z., Liu, Y., Lu, Z., Li, J., Hao, P., Zhang, Y., Zhang, F., et al. (2018). m6A facilitates hippocampus-dependent learning and memory through YTHDF1. *Nature 563*, 249-253.

Shi, J., Yang, C., Zhang, J., Zhao, K., Li, P., Kong, C., Wu, X., Sun, H., Zheng, R., and Sun, W. (2023a). NAT10 is involved in cardiac remodeling through ac4C-mediated transcriptomic regulation. *Circ Res 133*, 989-1002.

Shrestha, P., and Klann, E. (2022). Spatiotemporally resolved protein synthesis as a molecular framework for memory consolidation. *Trends Neurosci 45*, 297-311.

Sinclair, W.R., Arango, D., Shrimp, J.H., Zengeya, T.T., Thomas, J.M., Montgomery, D.C., Fox, S.D., Andresson, T., Oberdoerffer, S., and Meier, J.L. (2017). Profiling cytidine acetylation with specific affinity and reactivity. *ACS Chem Biol 12*, 2922-2926.

Srinivasan, R., Lu, T.Y., Chai, H., Xu, J., Huang, B.S., Golshani, P., Coppola, G., and Khakh, B.S. (2016). New Transgenic Mouse Lines for Selectively Targeting Astrocytes and Studying Calcium Signals in Astrocyte Processes In Situ and In Vivo. *Neuron 92*, 1181-1195.

Stern, L., and LH, S. (1978). The role of the minor base N4-acetylcytidine in the function of the Escherichia coli noninitiator methionine transfer RNA. *J Biol Chem 17,6132-6139.*

Steward, O., Wallace, C.S., Lyford, G.L., and Worley, P.F. (1998). Synaptic activation causes the mRNA for the IEG Arc to localize selectively near activated postsynaptic sites on dendrites. *Neuron 21*, 741-751.

Su, J., Huang, F., Tian, Y., Tian, R., Qianqian, G., Bello, S.T., Zeng, D., Jendrichovsky, P., Lau, C.G., and Xiong, W. (2023). Entorhinohippocampal cholecystokinin modulates spatial learning by facilitating neuroplasticity of hippocampal CA3-CA1 synapses. *Cell Rep 42,113467*.

Sutton, M.A., and Schuman, E.M. (2006). Dendritic protein synthesis, synaptic plasticity, and memory. *Cell 127*, 49-58.

Tan, G.H., Liu, Y.Y., Hu, X.L., Yin, D.M., Mei, L., and Xiong, Z.Q. (2011). Neuregulin 1 represses limbic epileptogenesis through ErbB4 in parvalbumin-expressing interneurons. *Nat Neurosci 15*, 258-266.

Tang, Y.P., Shimizu, E., Dube, G.R., Rampon, C., Kerchner, G.A., Zhuo, M., Liu, G., and Tsien, J.Z. (1999). Genetic enhancement of learning and memory in mice. *Nature 401*, 63-69.

Thalalla Gamage, S., Sas-Chen, A., Schwartz, S., and Meier, J.L. (2021). Quantitative nucleotide resolution profiling of RNA cytidine acetylation by ac4C-seq. *Nat Protoc 16*, 2286-2307.

Ting, A.K., Chen, Y., Wen, L., Yin, D.M., Shen, C., Tao, Y., Liu, X., Xiong, W.C., and Mei, L. (2011). Neuregulin 1 promotes excitatory synapse development and function in GABAergic interneurons. *J Neurosci 31*, 15-25.

Tsien, J.Z., Chen, D.F., Gerber, D., Tom, C., Mercer, E.H., Anderson, D.J., Mayford, M., Kandel, E.R., and Tonegawa, S. (1996). Subregion-and cell type–restricted gene knockout in mouse brain. *Cell 87*, 1317-1326.

Tullis, J.E., Larsen, M.E., Rumian, N.L., Freund, R.K., Boxer, E.E., Brown, C.N., Coultrap, S.J., Schulman, H., Aoto, J., Dell'Acqua, M.L., and Bayer, K.U. (2023). LTP induction by structural rather than enzymatic functions of CaMKII. *Nature 621*, 146-153.

Vorhees, C.V., and Williams, M.T. (2006). Morris water maze: procedures for assessing spatial and related forms of learning and memory. *Nat Protoc 1*, 848-858.

Wang, G., Zhang, M., Zhang, Y., Xie, Y., Zou, J., Zhong, J., Zheng, Z., Zhou, X., Zheng, Y., and Chen, B. (2022). NAT10-mediated mRNA N4-acetylcytidine modification promotes bladder cancer progression. *Clin Transl Med 12*, e738.

Wu, D., Bacaj, T., Morishita, W., Goswami, D., Arendt, K.L., Xu, W., Chen, L., Malenka, R.C., and Südhof, T.C. (2017). Postsynaptic synaptotagmins mediate AMPA receptor exocytosis during LTP. *Nature 544*, 316-321.

Wu, T., Hu, E., Xu, S., Chen, M., Guo, P., Dai, Z., Feng, T., Zhou, L., Tang, W., and Zhan, L. (2021). clusterProfiler 4.0: A universal enrichment tool for interpreting omics data. *Innovation (Camb) 2,100141*.

Xu, C., Zhang, J., Zhang, J., and Liu, B. (2021). SIRT7 is a deacetylase of N4-acetylcytidine on ribosomal RNA. *Genome Instab Dis 2*, 253-260.

Xu, T., Wang, J., Wu, Y., Wu, J.Y., Lu, W.C., Liu, M., Zhang, S.B., Xie, D., Xin, W.J., and Xie, J.D. (2023). Ac4C Enhances the Translation Efficiency of Vegfa mRNA and Mediates Central Sensitization in Spinal Dorsal Horn in Neuropathic Pain. *Adv Sci 10*, 2303113.

Yin, D.-M., Chen, Y.-J., Lu, Y.-S., Bean, J.C., Sathyamurthy, A., Shen, C., Liu, X., Lin, T.W., Smith, C.A., and Xiong, W.-C. (2013). Reversal of behavioral deficits and synaptic dysfunction in mice overexpressing neuregulin 1. *Neuron 78*, 644-657.

Yu, F., Zhang, Y., Cheng, C., Wang, W., Zhou, Z., Rang, W., Yu, H., Wei, Y., Wu, Q., and Zhang, Y. (2020). Poly (A)-seq: A method for direct sequencing and analysis of the transcriptomic poly (A)-tails. *PLoS One 15*, e0234696.

Yu, Q., Liu, Y.-Z., Zhu, Y.-B., Wang, Y.-Y., Li, Q., and Yin, D.-M. (2019). Genetic labeling reveals temporal and spatial expression pattern of D2 dopamine receptor in rat forebrain. *Brain Struct Funct 224*, 1035-1049.

Zhang, H.-L., Han, W., Du, Y.-Q., Zhao, B., Yang, P., and Yin, D.-M. (2021a). SRC3 acetylates calmodulin in the mouse brain to regulate synaptic plasticity and fear learning. *J Biol Chem* 297*,* 101044.

Zhang, H.-L., Zhao, B., Han, W., Sun, Y.-B., Yang, P., Chen, Y., Ni, D., Zhang, J., and Yin, D.-M. (2021b). Acetylation of calmodulin regulates synaptic plasticity and fear learning. *J Biol Chem* 297*, 101034*.

Zhang, H.-L., Zhao, B., Yang, P., Du, Y.-Q., Han, W., Xu, J., and Yin, D.-M. (2021c). Steroid receptor coactivator 3 regulates synaptic plasticity and hippocampus-dependent

memory. *Neurosci Bull 37*, 1645-1657.
Zhang, H.L., Hu, S., Yang, P., Long, H.C., Ma, Q.H., Yin, D.M., and Xu, G.Y. (2024). HDAC9-mediated calmodulin deacetylation induces memory impairment in Alzheimer's disease. *CNS Neurosci Ther 30*, e14573.
Zhang, M., Yang, K., Wang, Q.-H., Xie, L., Liu, Q., Wei, R., Tao, Y., Zheng, H.-L., Lin, N., and Xu, H. (2023a). The cytidine N-acetyltransferase NAT10 participates in peripheral nerve injury-induced neuropathic pain by stabilizing SYT9 expression in primary sensory neurons. *J Neurosci 43*, 3009-3027.
Zhang, W., Gao, J., Fan, L., Wang, J., He, B., Wang, Y., Zhang, X., and Mao, H. (2023b). ac4C acetylation regulates mRNA stability and translation efficiency in osteosarcoma. Heliyon *9*.
Zhang, Y., Liu, T., Meyer, C.A., Eeckhoute, J., Johnson, D.S., Bernstein, B.E., Nusbaum, C., Myers, R.M., Brown, M., Li, W., and Liu, X.S. (2008). Model-based Analysis of ChIP-Seq (MACS). *Genome Biol 9*, R137.
Zhou, H.-Q., Zhuang, L.-J., Bao, H.-Q., Li, S.-J., Dai, F.-Y., Wang, P., Li, Q., and Yin, D.-M. (2022). Olfactory regulation by dopamine and DRD2 receptor in the nose. *Proc Natl Acad Sci U S A 119*, e2118570119.
Zhuang, M., Geng, X., Han, P., Che, P., Liang, F., Liu, C., Yang, L., Yu, J., Zhang, Z., Dong, W., and Ji, S.-J. (2023). YTHDF2 in dentate gyrus is the m6A reader mediating m6A modification in hippocampus-dependent learning and memory. *Mol Psychiatry 28*, 1679-1691.

Methods

Animals

Adult male mice were used in this study to eliminate the possible effects of the hormone cycle. For stereotaxic injection of AAV, six-week-old mice were used. For behavioral analysis, nine-week-old mice were used. For ac4C dot-blots, LC-MS/MS, acRIP-seq, mice aged between nine and ten weeks were used. For immunofluorescence, western blots and electrophysiology, ten-week-old mice were used. Animals were housed in rooms at 23°C and 50% humidity in a 12 h light/dark cycle and with food and water available ad libitum. Animal experimental procedures were approved by the Institutional Animal Care and Use Committee of East China Normal University. The astrocyte-specific Cre (Aldh1l1-CreER) was purchased from Jackson lab (Stock No. 029655).

Generation of Nat10$^{Cre/+}$ knockin mice

The mouse Nat10 gene has 29 exons and the translational start codon (ATG) is localized in exon 2. We employed CRISPR/Cas9 technology in conjunction with homologous recombination to insert a Cre-WPRE-polyA expression cassette at the translational start

codon of the Nat10 gene in C57BL/6J mice. The process commenced with the synthesis of Cas9 mRNA and a guide RNA (gRNA) targeting the start codon of Nat10, with the gRNA sequence being 5′-catcatgaatcggaagaaggtgg-3′. A donor vector was then constructed using In-Fusion cloning, containing 2.6 kb 5′ and 3′ homology arms flanking the Cre-WPRE-pA cassette, designed for Cre recombinase expression, enhanced by the WPRE element and concluded with a polyadenylation signal. The cocktail of Cas9 mRNA, gRNA, and the donor vector was microinjected into fertilized C57BL/6J mouse embryos, leading to the birth of F0 generation mice. These mice were screened for the precise genomic integration of the cassette through PCR amplification and sequencing. Successful modifications were observed in F0 mice, which were subsequently bred with C57BL/6J mice to secure F1 progeny harboring the modification.

The resulting offspring were genotyped using PCR, with primers designed to detect the Cre within the Nat10 gene. The primers for genotyping wt Nat10 allele are as follows: forward: 5’tgtctttcctgtggtggtgt3’; reverse: 5’tgcgcactgaaaccctacaa3’. the primers for genotyping Nat10-cre allele are as follows: forward: 5’gaaatcatgcaggctggtgg3’; reverse: 5’aaagtcccggaaaggagctg3’. The PCR products for wt Nat10 and Nat10-Cre alleles were 392 and 393 bp, respectively.

Generation of Nat10$^{flox/flox}$ mice

The generation of Nat10$^{flox/flox}$ mice involved targeted modification of exon 4 within the Nat10 gene, utilizing CRISPR/Cas9-mediated gene editing. Two guide RNAs (gRNAs) were specifically designed to target and flank exon 4, enabling a precise floxed modification. The sequences for these gRNAs were as follows: gRNA1: 5′-tcagcagaccactttaaagatgg-3′ and gRNA2: 5′-tgcctgacatagtaaggtctggg-3′. Both Cas9 mRNA and gRNAs were produced through in vitro transcription techniques. A donor vector for homologous recombination was constructed using In-Fusion cloning. This vector included a 3.0 kb 5′ homology arm, a 0.7 kb loxp-flanked region (flox), and a 3.0 kb 3′ homology arm to ensure accurate genomic insertion at the Nat10 locus. The mixture of Cas9 mRNA and the two gRNAs was injected into the cytoplasm of one-cell stage embryos. These embryos were subsequently implanted into pseudopregnant females and carried to term.

The resulting offspring were genotyped using PCR, with primers designed to detect

the floxed exon 4 of Nat10 gene. The primers for genotyping the wt and floxed Nat10 allele are as follows: forward: 5'tgccgaggggatgtactcat3'; reverse: 5'agaaccccacgaactgtcct3'. The PCR products for wt Nat10 and floxed Nat10 allele were 302 and 356 bp, respectively.

Morris water maze (MWM)

The Morris Water Maze (MWM), a widely recognized method for assessing spatial learning and memory (Vorhees and Williams, 2006), was implemented with the following protocol: mice were acclimated to the testing environment over a period of three days through 10-minute daily handling sessions. To aid navigation, visual cues were strategically positioned around the perimeter of the maze. To ensure consistency and minimize the impact of external variables, all experimental sessions were conducted simultaneously each day. During the core phase of the experiment, spanning five days, mice were subjected to four trials daily. In each trial, they were released from different quadrants into the maze, with the escape platform being fixed in the first quadrant. A trial was deemed complete when a mouse successfully located the platform within a 60-second timeframe. If unsuccessful, the mouse was gently guided to the platform at the 60-second mark. The mice were handled for 10 minutes each day following the completion of the four trials. On the sixth day, a probe test was conducted, during which the platform was removed from the maze. During this test, mice were released from the third quadrant, and the number of times they crossed the former platform location during a 60-second trial was recorded as a measure of their retained spatial memory. Following the probe test, the mice were handled for a further 10 minutes before being returned to their home cages. After a two-week period in the home cages, the mice were subjected to the probe test again.

Chemical and reagents

All chemicals and reagents utilized in this study were of analytical grade. RNA was extracted using TRIzol® Reagent (15596-026, Invitrogen, Carlsbad, CA, USA) following the manufacturer's protocol. Chloroform and other general laboratory chemicals were obtained from Merck (109634, Darmstadt, Germany). The ACQUITY HSS T3 column (2.1×100 mm, 1.8 μm) for LC-MS/MS analysis was purchased from Waters Corporation (186008499, Milford, MA, USA). Phosphodiesterase was obtained

from Sigma (P3243-1VL, St. Louis, MO, USA). Nuclease P1 and alkaline phosphatase, used for RNA digestion, were obtained from Takara (2410A and 2250A). Hydroxylamine was from Aladdin Bio-Chem Technology Co., LTD (H164487). RNase inhibitor, which is critical for preserving RNA integrity during manipulations, was purchased from New England Biolabs (M0314S, NEB, CA, USA). Methylene blue, which is used for nucleic acid visualization, was obtained from Abcam (M9140). Poly-D-lysine was purchased from Sigma (Cat No. P1149). Tamoxifen was purchased from Sigma (Cat T5648).

Subcellular fractionation

The procedure of subcellular fractionation was adapted from the methodologies in our previous studies (Zhang *et al.*, 2021a; Zhang *et al.*, 2021b). Mouse brain tissues were processed starting with homogenization in Buffer A, which consists of 0.32 M sucrose, 1 mM $MgCl_2$, 1 mM PMSF, and a protease inhibitor cocktail to ensure comprehensive cell lysis while preserving protein integrity. The resultant homogenates were then filtered to remove cell debris and subsequently subjected to centrifugation at 500g for 5 minutes using a fixed-angle rotor. This step separates the homogenate into the pellet (P1) and supernatant (S1) fractions. The P1 fraction, containing primarily nuclei and unbroken cells, was further purified by resuspension in Buffer B (10 mM KCl, 1.5 mM $MgCl_2$, and 10 mM Tris-HCl at pH 7.4) followed by a repeat centrifugation under the same conditions to remove any remaining debris. The final pellet was resuspended in Buffer C (20 mM HEPES, pH 7.9, 25% glycerol, 1.5 mM $MgCl_2$, 1.4 M KCl, 0.2 mM EDTA, 0.2 mM PMSF, and 0.5 mM DTT), which is designed for nuclear protein extraction and incubated with agitation at 4 °C for 30 minutes to facilitate the release of nuclear proteins. A final centrifugation at 12,000g for 10 minutes was performed, and the supernatant, containing the nuclear protein fraction, was collected. The initial supernatant (S1), following the removal of P1, was further centrifuged at 10,000g for 10 minutes to partition it into the P2 fraction, which included the crude synaptosomes, and the cytosolic S2 fraction.

Western blot

Homogenates of hippocampus tissue were prepared in the RIPA buffer containing 50 mM Tris-HCl, pH 7.4, 150 mM NaCl, 2 mM EDTA, 1% sodium deoxycholate, 1%

SDS, 1 mM PMSF, 50 mM sodium fluoride, 1 mM sodium vanadate, 1 mM DTT, and protease inhibitors cocktails. All the protein samples were boiled at 100 °C water bath for 10 minutes before western blot. Homogenates were resolved on SDS/PAGE and then transferred to nitrocellulose membranes, which were incubated in the TBS buffer (0.1% Tween-20 and 5% milk) for 1 hour at room temperature followed by incubation of primary antibodies overnight at 4 °C. After washing, the membranes were incubated with HRP-conjugated secondary antibody in the same TBS buffer for 2 hours at room temperature. Immunoreactive bands were visualized by ChemiDocTM XRS + Imaging System (BIO-RAD) using enhanced chemiluminescence (Pierce) and analyzed with Image J (NIH). The following primary antibodies were used: anti-Histone H3 (1:1000, Cell Signaling, 9715), anti-SYN1 (1:1000, Cell Signaling, 2312), anti-α-tubulin (1:10000, Cell Signaling, 3873), anti-NAT10 (1:1000, Abcam, ab194297), anti-Acetyl-Histone H3 (1:1000, Cell Signaling, 9649), anti-ARC (1:1000, Proteintech, 66550-1-Ig), anti-PSD95 (1:1000, Cell Signaling, 3450), anti-PCAF (1:1000, Cell Signaling, 3378), and anti-GAPDH (1:5000, Abways, ab0037). The following secondary antibodies were used: HRP-conjugated secondary antibody (goat-anti-mouse, G-21040; goat-anti-rabbit, G-21234; 1:2000, Thermo Fisher).

Immunofluorescence

The mouse brains were fixed in 4% paraformaldehyde at room temperature for 1 hour and dehydrated in 20% sucrose at 4 ℃ overnight. Then the tissues were placed in an embedding mold and frozen in OCT media at 0 ℃. The embedded tissues were cut into slices with the thickness of 30 μm using a Leica microtome (CM3050S). The brain slices were permeabilized with 0.3% Triton-X 100 and 5% BSA in PBS and incubated with primary antibodies at 4 °C overnight. After washing with PBS for three times, samples were incubated with secondary antibodies for 2 hours at room temperature. Samples were mounted with Vectashield mounting medium (Vector Labs) and images were taken by Leica TCS SP8 confocal microscope. The following primary antibodies were used: rabbit anti-NeuN (1:1000, Abcam, ab177487), rabbit anti-Neurogranin (1:500, Abcam, ab217672). The following secondary antibodies were employed: Rabbit IgG (H+L) Highly Cross-Adsorbed Secondary Antibody (A32732, 1:500, Thermo Fisher). Unbiased stereology TissueFAX Plus ST (Tissue Gnostics, Vienna, Austria) was applied to count the number of Nat10-positive neurons. The detailed

methods for cell number counting is available on the website (https://tissuegnostics.com/products/single-cell-analysis/tissuequest).

Detection of ac4C and m6A modifications by LC-MS/MS

The analysis of LC-MS/MS followed previous studies with some modification (Arango *et al.*, 2018). Briefly, the RNA samples starting with 2 μg, were digested into nucleosides using alkaline phosphatase and nuclease P1 at 37°C for 3 hours. The digested samples were then subjected to chloroform extraction, with the aqueous phase being utilized for LC-MS/MS analysis in an AB SCIEX QTRAP 6500+ system, featuring an ACQUITY HSS T3 column (2.1×100 mm, 1.8 μm). Chromatographic separation was achieved with a mobile phase gradient of 2 mM ammonium bicarbonate in ultrapure water (A) and methanol (B), starting with 95% A and transitioning to 5% A over 8 minutes. A calibration curve spanning 0.0005 to 1000 pmol standard samples facilitated the accurate quantification of the epitranscriptomic modifications.

ac4C and m6A dot-blot

The total RNA of mouse hippocampus was extracted with Trizol according to the manufacturer's instructions. The polyA RNA was then purified using the Dynabeads™ polyA RNA purification kit (61006, Thermo Fisher). The dot-blot was performed according to the previous study (Zhang et al., 2023a). We used 0.5 μg of polyA RNA that fall in the linear range for each blot. For each HOM replicate, we purified 0.5 μg of polyA RNA from the hippocampus of one mouse. In contrast, for each SYN replicate, we purified 0.5 μg of polyA RNA from the hippocampus of five mice. In brief, the polyA RNA was denatured at 95 °C for 5 min using a heat block, immediately kept on ice for 1 min, loaded onto Amersham Hybond-N+ membrane and crosslinked with UV254 for 30 min. The membranes were blocked with 5% nonfat milk for 2 h at room temperature (RT), and incubated with the rabbit anti-m6A (1:2000, Synaptic System, #202003) or anti-ac4C antibody (1:500, Abcam, ab252215) at 4°C overnight. After wash with 0.05% PBST for three times, the membranes were incubated with the HRP-conjugated secondary antibody (goat-anti-rabbit, G-21234, 1:2000, Thermo Fisher) at RT for 2 h. The signals were visualized by ChemiDocTM XRS＋Imaging System (BIO-RAD) using ECL and analyzed with Image J (NIH). RNA loading was verified by staining the membranes with 0.2% methylene blue. The intensity of each dot was

normalized to total RNA.

Primary neuronal culture

The primary culture of mouse hippocampal neurons were performed according to our previous studies (Ting et al., 2011). Hippocampal explants from embryonic day 16 (E16) mouse embryos were digested with 0.125% trypsin solution for 30 min at 37°C, followed by trituration with pipette in plating medium (DMEM with 10% fetal bovine serum, 10% F-12, and 1% penicillin-streptomycin). The dissociated neurons were plated onto poly-D-lysine-coated coverslips at a density of 1×10^5 cells per 35 mm dish. Following a 4-hour incubation period, the plating medium was replaced with Neurobasal™ medium (Thermo Fisher, 21103049) supplemented with 2% B-27™ (Thermo Fisher, 17504044), 1% GlutaMax™ (Thermo Fisher, 35050061), and 1% penicillin-streptomycin (Invitrogen). Cytarabine (Sigma, C1768-100MG) was added after 2 days to a final concentration of 1 μM, to inhibit the proliferation of dividing non-neuronal cells. Half volume of the culture medium was replaced every 3-4 days with freshly prepared medium. The neurons were harvested at 14 days in vitro (DIV 14) for immunofluorescence experiments.

Chemical LTP (cLTP) and immunofluorescence

For cLTP, neurons were incubated with 300 μM glycine in a cell incubator set at 37°C with 5% CO_2 and 95% humidity for 3 minutes, followed by an additional 60 minutes without glycine at 37°C (Wu et al., 2017). Neurons were then fixed with 4% paraformaldehyde for 30 minutes on ice to preserve cell membranes. After washing with PBS, the neurons were penetrated with 0.3% Triton-X100 and blocked with 1% BSA in PBS for 30 min at RT. After that, neurons were incubated with primary antibodies (chicken anti-MAP2 antibody, 1:2000, Abcam, ab5392; mouse monoclonal anti-PSD95 antibody, 1:800, Abcam, ab192757; and rabbit monoclonal anti-NAT10 antibody, 1:800, Abcam, ab194297) overnight at 4°C. Neurons were then washed by PBS for three times before incubation with fluorescent secondary antibodies for 2 hours at 37°C. The following secondary antibodies were employed: Chicken IgY (H+L) Secondary Antibody (A-11039, 1:500, Thermo Fisher), Rabbit IgG (H+L) Cross-Adsorbed Secondary Antibody (A-21244, 1:500, Thermo Fisher), Rabbit IgG (H+L) Highly Cross-Adsorbed Secondary Antibody (A32732, 1:500, Thermo Fisher), and

Mouse IgG (H+L) Highly Cross-Adsorbed Secondary Antibody (A32727, 1:500, Thermo Fisher). After washing with PBS, the neurons were placed on mounting solution with DAPI (Beyotime, P0131). Confocal stacks were acquired from 3-6 individual fields on multiple coverslips per culture using a Leica SP8 confocal microscope. Two independent cultures were analyzed for each condition, including vehicle-treated control and glycine-treated neurons.

Regular acRIP-seq for HOM

The acRIP-seq was performed following the previous studies (Arango *et al.*, 2018; Thalalla Gamage et al., 2021). The total RNA was extracted from the HOM of mouse hippocampus using TRIzol, the quality of the RNA was evaluated through gel electrophoresis in order to ascertain its integrity and purity, and the concentration and purity of the RNA were detected. Total RNA samples, initially 100 μg, were treated with the rRNA depletion kit (New England Biolabs, Cat. No. E6310) to remove rRNA. After rRNA depletion, the RNA was subjected to immunoprecipitation using the anti-ac4C antibodies and the ac4C RIP kit (GenSeq, Cat No. GS-ET-005) according to the manufacturer's instructions. Briefly, total RNAs were randomly fragmented to ~200 nt by RNA Fragmentation Reagents (NEB, Cat No. M0348S). Protein A/G Dynabeads (Share-Bio, SB-PR001) were coupled to the anti-ac4C antibody by rotating at room temperature for 1 h. The RNA fragments were then incubated with the beads-linked anti-ac4C antibodies (2 μg) in the 100 μl acRIP buffer (PBS containing 1% Triton X-100, 2 mM BSA, and 1 mM RNase inhibitor) and rotated at 4°C for 4 h. After incubation, the RNA/antibody complexes were washed for four times with the acRIP buffer, and then RNAs were eluted by elution buffer (containing 0.1 M Glycine, 0.5% Triton X-100, PH 2.5-3.1) at room temperature for 10 minutes. Finally, add NaOH solution to adjust the pH of the elution product to neutral. Both the immunoprecipitated RNA and 1% input RNA are reverse transcribed with random hexamers, followed by RNA library preparation with Ultra™ II Directional RNA Library Prep Kit (New England Biolabs, Cat No. E7760) according to the manufacturer’s instructions.

The quality of RNA libraries were assessed using Agilent 2100 bioanalyzer and then subjected to the next-generation sequencing through the NovaSeq 6000 platform (Illumina). The quality of the sequencing data is measured using Q30 scores, and low-quality reads and 3' adaptors are removed using Cutadapt (v1.9.3). High-quality reads

are then aligned to the reference genome using Hisat2 (v2.0.4). Raw counts are generated using HTSeq (v0.9.1) and normalized using edgeR (v3.16.5). Gene expression was quantified by logged transcript per million mapped reads (log_2TPM).

Low-input acRIP-seq for SYN

The low-input acRIP-seq included some modifications, compared with the regular acRIP-seq. First, the RNA amount is relatively smaller (~ 1 µg, purified from the hippocampus of 10 mice) for low-input acRIP-seq, compared with regular acRIP-seq (~ 100 µg, purified from the hippocampus of 2 mice). Second, the total RNA purified from the SYN was not treated by the rRNA depletion kit before acRIP due to the low amount of rRNA in the SYN. Third, the RNA libraries for low-input acRIP-seq were generated by a different kit - SMARTer Stranded Total RNA-Seq Kit v2-Pico Input Mammalian (Clontech, Cat No. 050619). To increase the data reliability for low-input acRIP-seq, transcripts detected in at least two of the three databases of synaptic transcriptome (Cajigas et al., 2012; Hafner et al., 2019; Niu et al., 2023) were considered to be reliable mRNA expressed in the SYN.

Identification of ac4C peaks

Following RNA integrity assessments, acRIP enrichment verification, and library quality checks, raw sequencing reads from both acRIP and input samples underwent rigorous quality control. Initially, sequencing quality was evaluated using Q30 scores and FastQC to ensure base-level accuracy. Low-quality reads and 3' adaptor sequences were identified and removed using Cutadapt software (v1.9.3), resulting in high-quality clean reads for further analysis.

Post-alignment filtering was applied to exclude reads that mapped to mitochondrial DNA (chrM) and non-concordant mate pairs, which often arise from sequencing artifacts or alignment errors. The remaining clean reads were then aligned to the mouse genome (mm10) using Hisat2 software (v2.0.4), with parameters allowing a maximum of five mismatches per read to ensure alignment accuracy above 95%. Ensembl gene annotations (Release 75) were incorporated to guide accurate mapping to annotated regions. To account for transcript variability, canonical transcript sequences from the UCSC genome browser were used to generate a Bowtie2 index, enabling transcriptome mapping. Reads were aligned in local mode, which is well-suited for fragmented RNA

sequences.

Acetylation peaks (ac4C peaks) were identified using MACS software (v1.4.2) (Zhang et al., 2008), optimized for transcriptomic data. The shifting model and local lambda options were disabled to accommodate the unique characteristics of transcriptome data, and the genome size was set according to the total transcript base count. Input samples were used as controls to distinguish true ac4C-enriched peaks from background noise. The key aspect of this process was comparing the enrichment of clean reads between acRIP and input samples. Regions where acRIP samples exhibited significantly higher read enrichment compared to input samples were identified as potential acetylation peaks, reflecting areas where ac4C modifications are likely to occur. We established strict screening criteria in the peak calling process: adjusted $P < 0.05$ and a fold enrichment (FE) > 2. The ac4C peaks can be generated and visualized on the UCSC genome browser (https://genome.ucsc.edu/cgi-bin/hgGateway) using IGV (http://www.igv.org/). The FE was calculated as the ratio of acRIP to input.

$$FE = \frac{acRIP}{Input}$$

Sequence motif analysis

Sequence motifs were identified using HOMER (Heinz et al., 2010) and visualized using ggseqlogo package from R software. HOMER identifies motifs that are specifically enriched on learning set of sequences relative to control (e.g., peaks upstream and downstream sequences relative to the entire genome sequence) based primarily on the principle of ZOOPS scoring with hypergeometric enrichment.

Gene ontology and functional category analysis

Gene ontology (GO) analysis to detect enrichment for GO terms in differential acetylation genes in R using the clusterProfiler (Wu et al., 2021), and the possible roles of these differential acetylation genes were annotated according to MF, BP and CC. GO terms with a false-discovery rate adjusted P-value of < 0.05 were visualized using R scripts to plot. The R package clusterProfiler to visualize the genes composing KEGG pathways, and P-value < 0.05 was used as the threshold of significant enrichment.

Analysis of ac4C fold enrichment (FE) for individual mRNA

The fold enrichment of ac4C mRNA was reflected by the cumulative value of multiple

ac4C peaks from one particular mRNA molecule. Aggregating the cumulative sum of these peaks offers a more comprehensive overview of the total abundance of ac4C modifications across the mRNA molecule, avoiding the narrow focus on a potentially non-representative, single maximum modification site, similar with the previous study of m6A (Guca et al., 2024). Additionally, in instances where ac4C modifications on mRNA are more dispersed or present in low abundance, a single prominent peak may not be observable; instead, multiple low-abundance peaks might emerge. In such scenarios, the accumulation of multiple peaks can enhance detection sensitivity, better capture dynamic changes, and mitigate biases inherent in individual experiments. The following quantification index was used to calculate the ac4C levels of individual mRNA:

$$FE\ of\ ac4C = \Sigma peak\ (1 + 2 + 3 \ldots\ldots + n)$$

Analysis of ac4C fold change (FC) for individual mRNA

The fold change of ac4C mRNA is representative of the degree of change in the overall acetylation level of mRNA in the learning group (L) compared with the control group (C). To prevent a value of 0 in the denominator in the FC calculation, we added 1 to the FE of ac4C. The FC of ac4C mRNA was calculated using the following quantification index:

$$FC\ of\ ac4C = \frac{(FE\ of\ ac4C + 1)\ in\ L}{(FE\ of\ ac4C + 1)\ in\ C}$$

Analysis of PPI network

The STRING (https://string-db.org/) (version 12.0) knowledge base was used to create a protein-protein interaction (PPI) network. The PPI network was generated with a confidence score of 0.7 and visualized using Cytoscape (version 3.10.1). Molecular Complex Detection (MCODE) (v2.0.3) algorithm was employed to identify the components of the densely connected network.

The following software and algorithms were used for the quantification and statistical analysis of ac4C epitranscriptome.

Software and algorithms, application, authors		
R v4.3.2	Statistical computing and graphics.	R Core Team. R Foundation for

		Statistical Computing 2023.
Python v3.11	Object-oriented programming language.	Van R et al. CreateSpace 2009.
ggplot2	Creating graphics, based on The Grammar of Graphics.	Hadley W et al, Springer-Verlag New York 2016.
ggseqlogo	Generating publication-ready sequence logos using ggplot2.	Wagih et al. Bioinformatics 2018.
tidyverse	Collection of R packages designed for data science.	Wickham et al. Journal of Open Source Software 2019.
ComplexHeatmap	Arrange multiple heatmaps and supports annotation graphics.	Gu Z et al. Bioinformatics 2016.
HOMER v4.11	Motif Discovery and gene sequencing analysis.	Heinz S et al. Mol Cell 2010.
bedtools	Compare large sets of genomic features.	Aaron Q et al. Bioinformatics 2010.
cutadapt v1.9.3	Remove sequencing data adaptor.	Martin M. EMBnet 2011.
Hisat2 v2.04	Mapping sequencing reads to a single reference genome.	Zhang Y et al. Genome Research 2021.
MACS v1.4.2	Identifying transcript factor binding sites.	Yong Z et al. Genome Biology 2008.
Pandas v2.1.4	Cleaning data.	The pandas development team. Zenodo 2020.
IGV	Interactive genome visualization application.	James T et al. Bioinformatics 2023.
HTSeq (v0.9.1)	Analysing high-throughput sequencing data.	Simon A et al. Bioinformatics 2014.
edgeR (v3.16.5)	Empirical analysis of digital gene expression data.	McCarthy DJ et al. Nucleic Acids Research 2012.
CIBERSORT	Cell-type identification by estimating relative subsets of RNA transcripts.	Aaron M et al. Nature methods 2015.

1211

Identification of relative abundance of genes in different cell types

We applied the CIBERSORT (Cell-type Identification by Estimating Relative Subsets of RNA Transcripts) algorithm (Newman et al., 2015) in R to determine the enriched cell types where the genes of NASA mRNAs were expressed. To construct the reference gene signature matrices, we used Dataset C from McCarroll Lab (http://dropviz.org/) (Saunders *et al.*, 2018) to extract gene expression features for various hippocampal cell types, including excitatory neurons, inhibitory neurons, astrocytes, and microglia. These reference matrices were then used to deconvolve the gene expression data and estimate the contributions from each cell type.

RT-qPCR

The cDNA was obtained through reverse transcription using the HiScript III RT SuperMix for qPCR kit (Vazyme, R323-01), followed by amplification using the ChamQ Universal SYBR qPCR Master Mix kit (Vazyme, Q711-02). Gene expression levels measured with RT-PCR were normalized to Gapdh. The primers used in qPCR for this study were as follows: Gapdh-forward, 5'gggtgtgaaccacgagaaat3'; Gapdh-reverse 5'actgtggtcatgagcccttc3'; Arc-forward, 5'ggagggaggtcttctaccgtc3'; Arc-reverse 5'cccccacacctacagagaca3'; Grin2b-forward, 5'ctggtgaccaatggcaagcatg3'; Grin2b-reverse, 5'ggcacagagaagtcaaccacct3'; Camk2α-forward, 5'agccatcctcaccactatgctg3'; Camk2α-reverse 5'gtgtcttcgtcctcaatggtgg3'.

Stereotaxic injection of AAV into mouse hippocampus

AAV2/9-Syn1-EGFP and AAV2/9-Syn1-EGFP-P2A-Cre were generated by Hanbio Technology (Shanghai) Corp., Ltd., with a titer of 10^{12}/μl. We injected 0.3 μl AAV into each side of the mouse hippocampus. Six-week-old Nat10$^{flox/flox}$ mice received an intraperitoneal injection of alphaxalone at a dosage of 40 mg/kg for anesthesia and then were immobilized in a stereotaxic frame provided by RWD Life Science. Similarly, AAV2/9-CAG-DIO-EGFP, generated by Hanbio Technology (Shanghai) Corp., Ltd., with a titer of 10^{12}/μl, was injected into the hippocampus of seven-week-old Nat10$^{Cre/+}$ and ALDH1L1$^{Cre/ERT2}$ mice. The AAVs were delivered into mouse hippocampus through a Stoelting stereotaxic injector at a flow rate of 0.1 μl/min. The precise coordinates for the stereotaxic injection were set to anteroposterior (AP) −2.3 mm, dorsoventral (DV) −1.8 mm, and mediolateral (ML)±1.75 mm, relative to the Bregma.

To induce Cre enzyme expression, mice were fed a custom-made tamoxifen-infused diet over a period of one week, with the administration occurring on an intermittent schedule (Tan et al., 2011).

Electrophysiological recording

Hippocampal slices were prepared as previously described (Yin et al., 2013). Briefly, mice (10 weeks old, male) were decapitated and transverse hippocampal slices (400 μm) were prepared using a Vibroslice (VT 1000S; Leica) in ice-cold ACSF. For field potential recording, the same ACSF was used for slice preparation and recording: 120 mM NaCl, 2.5 mM KCl, 1.2 mM NaH_2PO_4, 2.0 mM $CaCl_2$, 2.0 mM $MgSO_4$, 26 mM $NaHCO_3$ and 10 mM glucose. After sectioning, hippocampal slices were allowed to recover in the chamber for 30 min at 34°C and then for a further 2-8 h at room temperature (25 ± 1°C). All solutions were saturated with 95% O_2/5% CO_2 (vol/vol). The slices were placed in the recording chamber, which was superfused (3 mL/min) with ACSF at 32-34°C. fEPSPs were evoked in the CA1 stratum radiatum by stimulating the SC with a bipolar stimulating electrode (FHC) and recorded in current clamp using a HEKA EPC 10 amplifier (HEKA Elektronik) with ACSF-filled glass pipettes (1-3 MΩ). Test stimuli consisted of monophasic 100-μs pulses of constant current (intensity adjusted to produce 25% of the maximum response) at a frequency of 0.033 Hz. The strength of synaptic transmission was determined by measuring the initial amplitude of fEPSPs. L-LTP was induced by 4 trains of 100 Hz stimuli of 50 pulses each at 100 Hz, 10 s apart, at the same intensity as the test stimulus. The level of E-LTP / L-LTP was determined at an average of 55-60 / 115-120 min after HFS stimulation. To study glutamatergic transmission at SC-CA1 synapses, we recorded fEPSP input/output (I/O) curves at SC-CA1 synapses. To construct an I/O curve, fEPSPs were evoked by a series of incremental intensities (0.02-0.2 mA in 0.02 mA increments, 100 μs duration, at 0.033 Hz). Whole-cell patch-clamp recordings from CA1 neurons were visualized with infrared optics using an upright microscope equipped with a 40× water-immersion objective (BX51WI; Olympus) and an infrared-sensitive CCD camera. To analyze the intrinsic excitability of CA1 pyramidal neurons,

the current clamp was used and neurons were held at 0 pA and then injected with step currents (duration: 500 ms; increments: 20 pA; range: -100 to 400 pA; interval: 10 s). The input-output relationship was determined by plotting the injected currents against the number of action potentials. All data were acquired at a sampling rate of 10 kHz using PATCHMASTER version 2 x 90.1 software (HEKA Elektronik) and filtered off-line at 1 kHz.

Generation and use of the ac4C website

The ac4Catlas website was constructed using HTML (a scripting language for front-end development), PHP (a scripting language for backend development), and MySQL (a structured query language for data operation). All the website codes were deployed in a Linux server equipped with Centos environment. The raw data, processed data and annotated files were stored in "Data Downloads" section. JBrowse (https://jbrowse.org) was integrated to visualize the ac4C epitranscriptomic data on genomic regions of interest. Briefly, ac4Catlas provides user-friendly interactive interfaces which allow researchers to freely browse and perform extended operations, such as searching, comparing, and downloading. Besides, the browse module stores detailed information of samples and corresponding datasets as well as ac4C levels of mRNA and differentially acetylated regions between groups.

Statistical analysis

The cumulative distribution curve was analyzed by Kolmogorov-Smirnov test in R. The statistical analysis of percentage of ac4C summits occurring within CDS or UTRs was performed by chi-square test in R. The regular quantification data were shown as mean ± SEM unless otherwise mentioned. The sample size justification was based on the previous studies and met the requirement of statistics power. For normally distributed data with 1 experimental variable, statistical analyses were performed by parametric analysis: unpaired (two-tailed) student's t-test for two groups and one-way ANOVA with the Tukey's multiple-comparison test for 3 groups. Data with >1 experimental

variable were evaluated by two-way ANOVA, with post hoc Tukey, Dunnett or Sidak's multiple-comparison tests. All these statistical analyses were performed by the software of GraphPad Prism 10. Statistically significant difference was indicated as follows: **** $P < 0.0001$, *** $P < 0.001$, ** $P < 0.01$ and * $P < 0.05$.

Acknowledgements

We thank CloudSeq Inc. (Shanghai, China) for providing us with technical support on acRIP-seq. This work was supported by STI2030-Major Projects (Grant No. 2021ZD0202500) and the National Natural Science Foundation of China (Grant No. 32300560), and the Fundamental Research Funds for the Central Universities (Grant No. YBNLTS2022-011).

Author contributions

H.-Q.Z. and H.J. performed biochemical and behavioral analysis, H.-Q.Z., J.-W.Z., and Z.Z. analyzed the data, W.-P.L. and Y.-Y.D. performed electrophysiology. S.C. generated the ac4C website, D.-M.Y. conceived the idea, supervised the work and wrote the paper. All authors approved the final version of the manuscript.

Competing interests

The authors declare no competing interests.

Data and materials availability

All data are available in the main text, supplementary or source data files. The original data of acRIP-seq is accessible via the website (http://ac4Catlas.com/) or GEO database (GSE261922). The source data files are provided with the paper, which contain high-resolution figures, uncropped western blot images, and original statistical data. All unique materials used are readily available from the corresponding author upon reasonable requests.

Code availability

Custom code used in this paper is available at https://github.com/YinDMlab/ac4CRIP-seq-analysis.

Figures and Legends

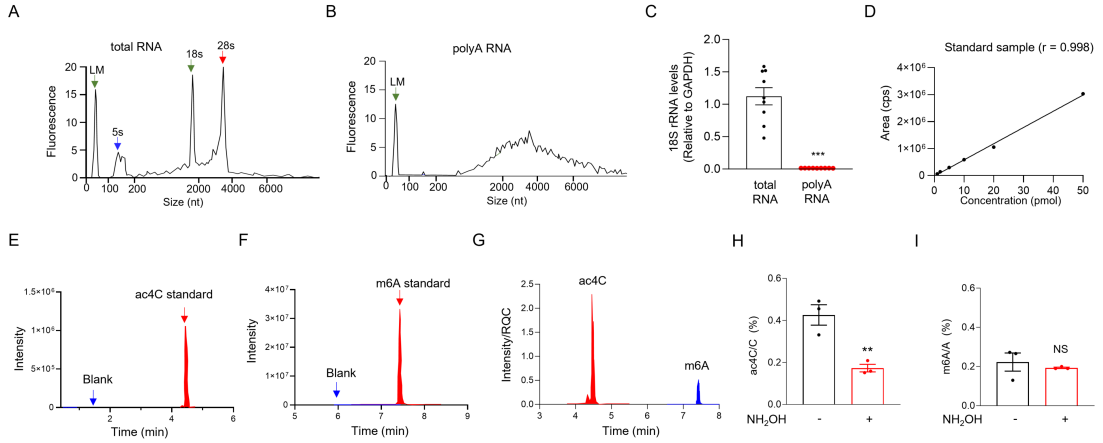

Figure 1 The presence of ac4C modification in PolyA RNA of mouse hippocampus. **A-B**, Verification of the purity of PolyA RNA through the bioanalyzer profiling. The x-axis represents the size of nucleotides, and the y-axis represents the fluorescent signal from the bioanalyzer. A, total RNA. B, PolyA RNA. **C**, Diminished levels of 18S rRNA in the polyA RNA samples, compared with total RNA samples, which was revealed by RT-qPCR analysis. The levels of 18S rRNA were normalized by that of Gapdh. *** $P < 0.0001$, two-tailed t-test, n = 6 biological replicates. **D**, Standard ac4C curve for LC-MS/MS analysis. The standard samples consisting of varying concentrations of ac4C nucleotide (1 pmol, 2 pmol, 5 pmol, 10 pmol, 20 pmol, and 50 pmol) were analyzed by MS/MS to generate a calibration curve. The x-axis represents the concentration of the ac4C standard samples, and the y-axis represents the signal intensity from the MS/MS analysis. The linear regression analysis yielded a correlation coefficient (r) of 0.998, indicating a strong linear relationship between ac4C concentration and LC-MS/MS signal. **E-F**, The chromatograms of blank samples and ac4C (E) and m6A (F) standards in the LC-MS/MS analysis. **G**, The representative chromatograms of ac4C and m6A peaks identified in the polyA RNA purified from the HOM of mouse hippocampus. **H**, Reduction of ac4C levels by the chemical deacetylation protocol. The stoichiometry

levels of ac4C in polyA RNA from control and NH_2OH-treated samples were quantified. ** P = 0.008, two-tailed t-test, n = 3 biological replicates. **I**, Unchanged m6A levels by the chemical deacetylation protocol. The stoichiometry levels of m6A in polyA RNA from control and NH_2OH-treated samples were quantified. NS, not significant, two-tailed t-test, n = 3 biological replicates. Quantification data are expressed as mean ± SEM.

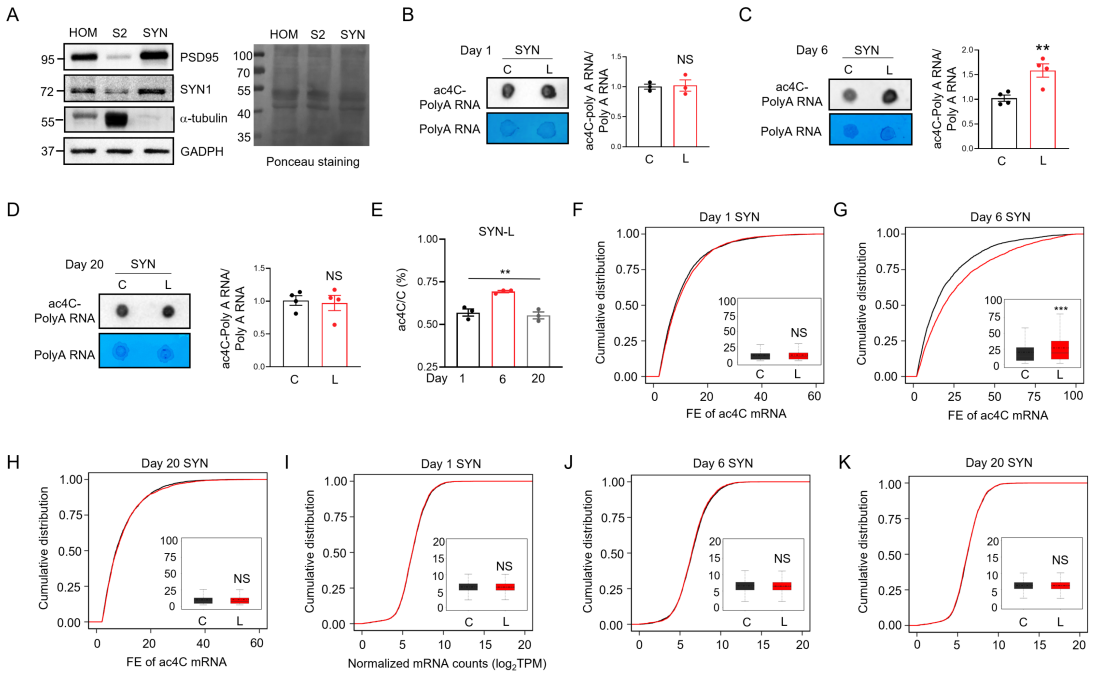

Figure 2 Increased mRNA acetylation in the SYN of mouse hippocampus after learning and memory. A, The purified synaptosomes (SYN) of mouse hippocampus expressed high levels of PSD95 and synapsin 1 (SYN1), two synaptic protein markers, but very low levels of α-tubulin, a cytoplasmic protein marker. The homogenates (HOM), cytoplasm (S2) and SYN of mouse hippocampus were subjected to western blots with the indicated antibodies. Left panel, representative images of western blots; right panel, Ponceau staining to show equal protein loading. **B,** Acetylation of polyA RNA was not altered in SYN of mouse hippocampus at day 1. The polyA RNA purified from the SYN of control and learning mice at day 1 after MWM training were subjected to ac4C dot-blots and methylene blue staining. Left, the representative images; right, quantification data. NS, not significant, two-tailed t-test, n = 3 biological replicates. Data were normalized by controls. **C,** Acetylation of polyA RNA was increased in the

SYN of mouse hippocampus at day 6. The polyA RNA purified from the SYN of control and learning mice at day 6 after MWM training were subjected to ac4C dot-blots and methylene blue staining. Left, the representative images; right, quantification data. ** P = 0.0093, two-tailed t-test, n = 4 biological replicates. Data were normalized by controls. **D**, Acetylation of polyA RNA was not altered in the SYN of mouse hippocampus at day 20. The polyA RNA purified from the SYN of control and learning mice at day 20 after MWM training were subjected to ac4C dot-blots and methylene blue staining. Left, the representative images; right, quantification data. NS, not significant, two-tailed t-test, n = 4 biological replicates. Data were normalized by controls. **E,** Acetylation of mRNA in the SYN was increased during memory formation but returned to normal levels after forgetting. The stoichiometry levels of ac4C of polyA RNA purified from the learning (L) mice were shown at days 1, 6 and 20 after MWM training. ** P = 0.0023, one-way-ANOVA, n = 3 biological replicates. **F-H**, Acetylation of mRNA was increased after memory formation but returned to normal levels after forgetting in the SYN of mouse hippocampus. Shown are cumulative distribution curves of FE of ac4C mRNA purified from the SYN of control (C) and learning (L) mice at days 1 **(**F), 6 (G), and 20 (H) after MWM training. The FE of ac4C mRNA was quantified in the quartile boxplots, where the solid line in the box is the median and the dashed line is the mean, where the maximum and minimum values are identified. NS, not significant, *** adj-P = 9.9814e-13, Kolmogorov-Smirnov test. **I-K,** The total mRNA levels were not significantly altered in the SYN of mouse hippocampus during learning and memory. Shown are cumulative distribution curves of normalized mRNA counts for SYN in control (C) and learning (L) mice at days 1 (I), 6 (J) and 20 (K) after MWM training. The normalized mRNA counts were quantified in the quartile boxplots, where the solid line in the box is the median and the dashed line is the mean, where the maximum and minimum values are identified. NS, not significant, Kolmogorov-Smirnov test. C, control; L, learning. FE, Fold Enrichment. Quantification data are expressed as mean ± SEM.

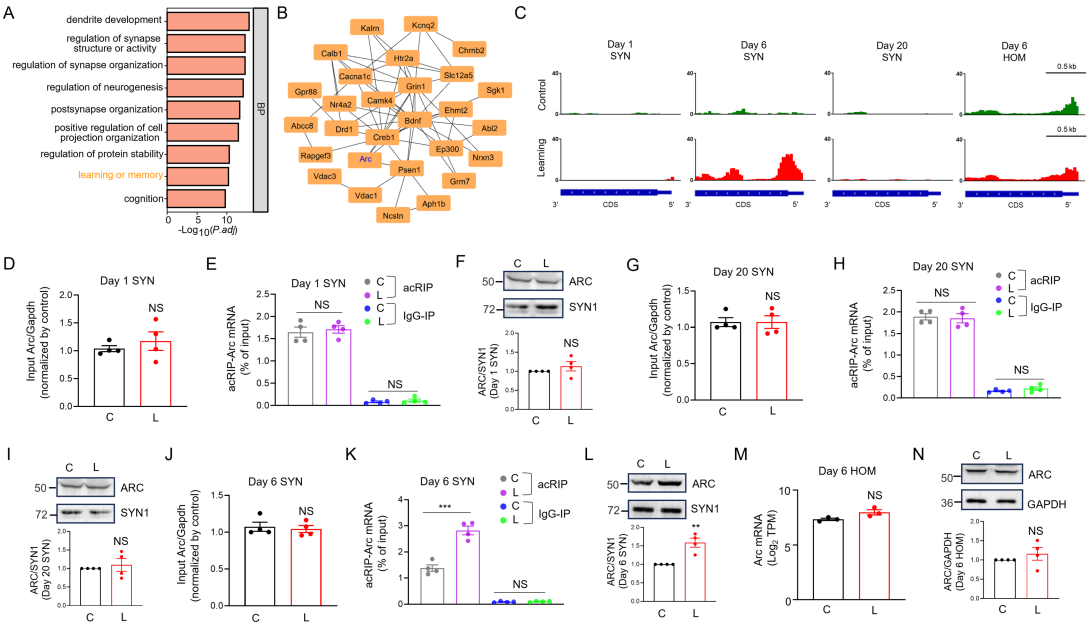

Figure 3 A representative LISA mRNA for Arc. A, The biological processes (BP) in which LISA mRNAs are significantly overrepresented. The x-axis represents the negative logarithm of the adjusted p-value, reflecting the significance of the enrichment, while the y-axis shows the biological processes. **B,** The protein-protein interaction (PPI) network of LISA mRNA implicated in the BP of learning or memory. P < 1.0e-16, Hypergeometric Test**. C**, Increased ac4C modification of Arc in the SYN rather than in the HOM at day 6. Also note the unaltered ac4C Arc mRNA at days 1 or 20 in the SYN. Shown are the IGV maps of the ac4C peaks from the CDS region of Arc mRNA. The ac4C peaks were represented by acRIP/input (See details in the Method). **D**, **G**, The Arc mRNA levels from the input of SYN were not altered at days 1 (D) or 20 (G) after MWM training. The RNA purified from the SYN was subjected to the RT-qPCR analysis. NS, not significant, two-tailed t-test, n = 4 biological replicates. The levels of Arc mRNA were normalized by that of Gapdh in each sample, and then the ratio of Arc to Gapdh were normalized by controls. **E**, **H**, The ac4C modification of Arc mRNA was not altered in the SYN at days 1 (E) or 20 (H) after MWM training. The RNA purified through the acRIP and IgG-IP products of SYN was subjected to the RT-qPCR analysis. NS, not significant, two-way-ANOVA followed by Tukey's multiple comparison test, n = 4 biological replicates. Data were normalized by input. **F**, **I**, The protein levels of ARC did not change in the SYN at days 1 (F) or 20 (I) after MWM training. Top,

representative western blot images; bottom, quantification data. NS, not significant, two-tailed t-test, n = 4 biological replicates. The protein levels of ARC were normalized by that of SYN1 in each sample, and then the ratio of ARC to SYN1 were normalized by controls. **J**, The Arc mRNA levels from the input of SYN were not altered at day 6 after MWM training. The RNA purified from the SYN was subjected to the RT-qPCR analysis. NS, not significant, two-tailed t-test, n = 4 biological replicates. The levels of Arc mRNA were normalized by that of Gapdh in each sample, and then the ratio of Arc to Gapdh were normalized by controls. **K**, The ac4C modification of Arc mRNA was significantly increased in the SYN at day 6 after MWM training. The RNA purified from the acRIP and IgG-IP products of SYN was subjected to the RT-qPCR analysis. *** $P < 0.001$, two-way-ANOVA followed by Tukey's multiple comparison test, n = 4 biological replicates. Data were normalized by input. **L**, The protein levels of ARC were significantly increased in the SYN at day 6 after MWM training. Top, representative western blot images; bottom, quantification data. ** $P = 0.0032$, two-tailed t-test, n = 4 biological replicates. The protein levels of ARC were normalized by that of SYN1 in each sample, and then the ratio of ARC to SYN1 were normalized by controls. **M**, The Arc mRNA levels from the HOM were not altered at day 6 after MWM training. The Arc mRNA levels were revealed by the $\log_2$TPM from the next-generation sequencing of the HOM RNA. NS, not significant, two-tailed t-test, n = 3 biological replicates. **N**, The protein levels of ARC did not change in the HOM at day 6 after MWM training. Top, representative western blot images; bottom, quantification data. NS, not significant, two-tailed t-test, n = 4 biological replicates. The protein levels of ARC were normalized by that of GAPDH in each sample, and then the ratio of ARC to GAPDH were normalized by controls. C, control; L, learning. Quantification data are expressed as mean ± SEM.

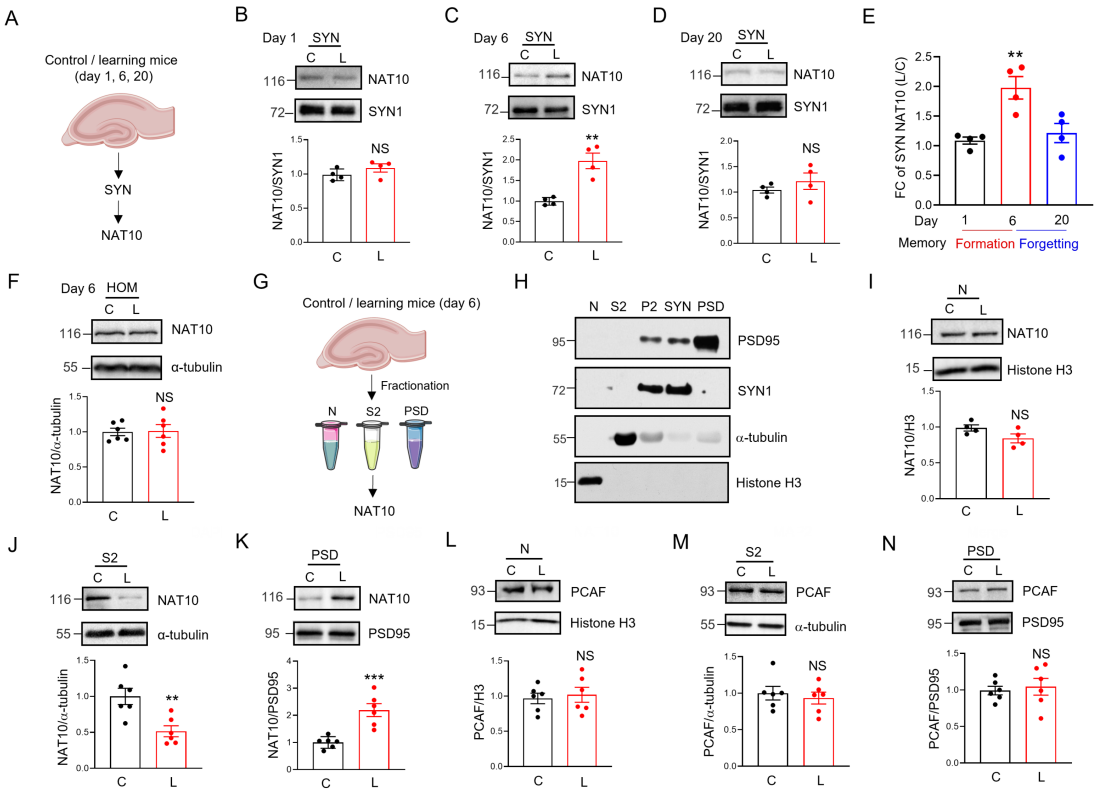

Figure 4 Increased NAT10 proteins in the SYN of mouse hippocampus after learning and memory. A, Experimental design. The SYN fractions were purified from the hippocampus of control and learning mice at days 1, 6 and 20. The NAT10 protein levels in the SYN were then assessed by western blots. **B-D**, Protein levels of NAT10 were increased in the SYN after memory formation but returned to normal levels after forgetting. The SYN proteins from control and learning mice at days 1 (B), 6 (C), and 20 (D) were subjected to western blots with the indicated antibodies. The protein levels of NAT10 were normalized by that of SYN1 in each sample, and then the ratio of NAT10 to SYN1 was normalized by controls. Top, representative western blot images; bottom, quantification data. NS, not significant, ** P = 0.0023, two-tailed t-test, n = 4 biological replicates. **E**, The fold change (FC) of NAT10 proteins in panel B to D was quantified. ** P = 0.0043, one-way-ANOVA, n = 4 biological replicates. **F**, Protein levels of NAT10 were not altered in the HOM at day 6. The HOM proteins from control and learning mice at day 6 were subjected to western blots with the indicated antibodies. Top, representative western blot images; bottom, quantification data. NS, not significant, two-tailed t-test. Data were normalized by controls, n = 6 biological replicates at each

1465 condition. The protein levels of NAT10 were normalized by that of α-tubulin in each
1466 sample, and then the ratio of NAT10 to α-tubulin was normalized by controls. **G**,
1467 Experimental design. Proteins were extracted from nucleus (N), cytoplasm (S2), and
1468 postsynaptic density (PSD) of control and learning mouse hippocampus at day 6, and
1469 then NAT10 protein levels were assessed by western blots. **H**, Expression of different
1470 protein markers in the nuclear (N), cytoplasmic (S2), P2, SYN, and PSD fractions of
1471 mouse hippocampus. Shown are representative images of western blots. Protein
1472 samples purified from different subcellular fractions of mouse hippocampus were
1473 subjected to western blots with the indicated antibodies. **I**, Protein levels of NAT10
1474 were not altered in the nuclear fraction of mouse hippocampus after memory formation.
1475 The nuclear protein samples from control and learning mice at day 6 were subjected to
1476 western blots with the indicated antibodies. Top, representative western blot images;
1477 bottom, quantification data. NS, not significant, two-tailed t-test, n = 4 biological
1478 replicates. The protein levels of NAT10 were normalized by that of Histone H3 proteins
1479 in each sample, and then the ratio of NAT10 to Histone H3 was normalized by controls.
1480 **J**, Protein levels of NAT10 were significantly reduced in the S2 fraction of mouse
1481 hippocampus after memory formation. The cytoplasmic protein samples from control
1482 and learning mice at day 6 were subjected to western blots with the indicated antibodies.
1483 Top, representative western blot images; bottom, quantification data. ** P = 0.0052,
1484 two-tailed t-test, n = 6 biological replicates. The protein levels of NAT10 were
1485 normalized by that of α-tubulin in each sample, and then the ratio of NAT10 to α-
1486 tubulin was normalized by controls. **K**, Protein levels of NAT10 were significantly
1487 increased in the PSD fraction of mouse hippocampus after memory formation. The PSD
1488 protein samples from control and learning mice at day 6 were subjected to western blots
1489 with the indicated antibodies. Top, representative western blot images; bottom,
1490 quantification data. *** P = 0.0008, two-tailed t-test. n = 6 biological replicates. The
1491 protein levels of NAT10 were normalized by that of PSD95 in each sample, and then
1492 the ratio of NAT10 to PSD95 was normalized by controls. **L-N**, Protein levels of PCAF
1493 were not altered in the nuclear (L), S2 (M), or PSD fraction (N) of mouse hippocampus

after memory formation. The protein samples purified from the different subcellular fractions of the hippocampus of control and learning mice at day 6 were subjected to western blots with the indicated antibodies. Top, representative western blot images; bottom, quantification data. NS, not significant, two-tailed t-test, n = 6 biological replicates. The protein levels were normalized by the protein markers in different subcellular fractions and then were normalized by controls. C, control; L, learning. Quantification data are expressed as mean ± SEM.

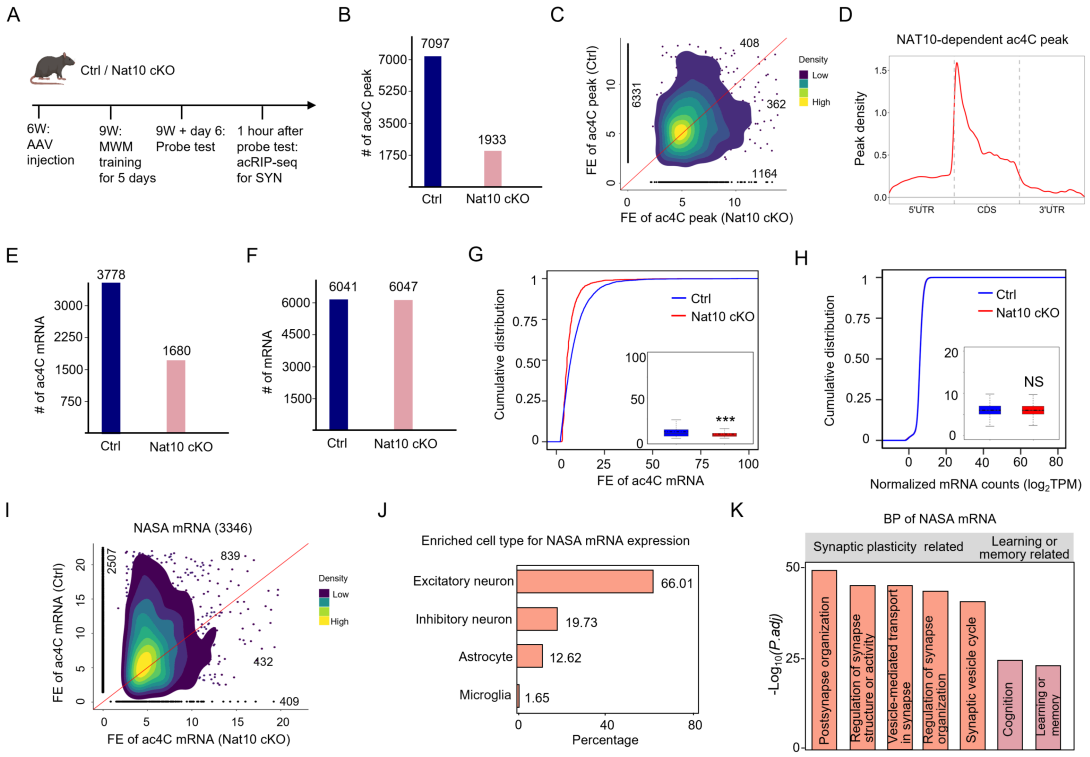

Figure 5 NAT10-dependent of ac4C mapping in the SYN of learning mice. A, Experimental design. Three weeks after AAV injection, the control (Ctrl) and Nat10 conditional knockout (cKO) mice were subjected to MWM training and probe test, and then the SYN fractions were purified from hippocampal tissues for low-input acRIP-seq. **B**, Reduction of ac4C peak number in the SYN of Nat10 cKO mice, compared with controls. 7097 and 1933 ac4C peaks were identified in the SYN of control and Nat10 cKO mice, respectively. **C**, Definition of NAT10-dependent ac4C peaks through acRIP summits displaying higher FE values in control relative to Nat10 cKO mice. Shown are the density scatter plot of ac4C peaks. Each dot represents an ac4C peak. 6631 ac4C

peaks are specifically identified in the SYN of control but not Nat10 cKO mice. The FE of 408 ac4C peaks was higher in the SYN of control mice than Nat10 cKO mice. **D**, NAT10-dependent ac4C peaks are predominantly located in the CDS region of mRNA. The plot shows the density of ac4C peaks along various mRNA regions, including the 5'UTR, CDS, and 3'UTR. **E**, Reduction of ac4C mRNA number in the SYN of Nat10 cKO mice, compared with controls. 3778 and 1680 ac4C mRNAs were identified in the SYN of control and Nat10 cKO groups, respectively. **F**, Similar mRNA numbers identified in the SYN of control and Nat10 cKO mice. 6041 and 6047 mRNAs were identified in the SYN of control and Nat10 cKO mice, respectively. **G**, Acetylation of mRNA in the SYN of Nat10 cKO mice was significantly reduced, compared with controls. Shown are cumulative distribution curves of FE of ac4C mRNA purified from the SYN of control and Nat10 cKO mice at day 6 after MWM training. The FE of ac4C mRNA was quantified in the quartile boxplots, where the solid line in the box is the median and the dashed line is the mean, where the maximum and minimum values are identified. *** adj-P = 1.20076e-12, Kolmogorov-Smirnov test. **H**, The total mRNA levels were not significantly altered in the SYN of Nat10 cKO mice, compared to controls. Shown are cumulative distribution curves of normalized mRNA counts for SYN in control and Nat10 cKO mice at day 6 after MWM training. The normalized mRNA counts were quantified in the quartile boxplots, where the solid line in the box is the median and the dashed line is the mean, where the maximum and minimum values are identified. NS, not significant, Kolmogorov-Smirnov test. **I**, Definition of NAT10-dependent synaptic ac4C (NASA) mRNA through acRIP summits displaying higher FE values in control relative to Nat10 cKO mice. Shown are the density scatter plot of ac4C mRNA. Each dot represents an ac4C mRNA. 2507 ac4C mRNAs are specifically identified in the SYN of control but not Nat10 cKO mice. The FE of 839 ac4C mRNA was higher in the SYN of control mice than Nat10 cKO mice. **J**, The expression of NASA mRNA is mostly enriched in excitatory neurons of mouse hippocampus. Shown are the percentage of NASA mRNA whose expression was relatively enriched in different cell types of mouse hippocampus through analysis of the single-cell RNA-

sequencing dataset (http://dropviz.org). **K**, The biological processes (BP) in which NASA mRNAs are significantly overrepresented. The y-axis represents the negative logarithm of the adjusted p-value, reflecting the significance of the enrichment. Quantification data are expressed as mean ± SEM.

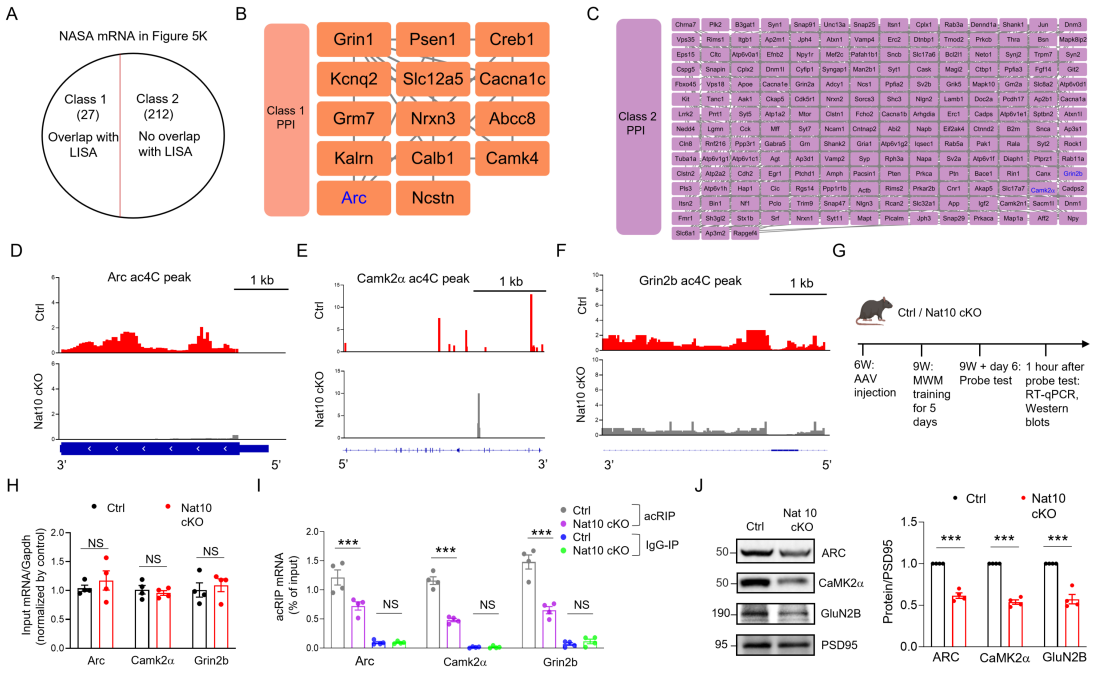

Figure 6 Reduction of ac4C modification and protein levels of Arc, Camk2α and Grin2b in the SYN of Nat10 cKO mice, compared with controls. A, Classification of NASA mRNAs overrepresented in the BP related to synaptic plasticity and learning or memory (Figure 5K). 27 NASA mRNAs overlap with LISA mRNAs, which were named class 1 mRNA. In contrast, 212 NASA mRNAs do not overlap with LISA mRNAs, which were named class 2 mRNA. **B**, **C**, The protein-protein interaction (PPI) network of class 1 (B) and 2 (C) mRNA. Class 1: P < 3.9e-11; Class 2: P < 1.0e-16, Hypergeometric test. **D-F**, Reduced ac4C modification of Arc (D), Camk2α (E), and Grin2b (F) mRNA in the SYN of Nat10 cKO mice at day 6, compared with controls. Shown are the IGV maps of the ac4C peaks from the 3' UTR to the 5' UTR of transcripts. The ac4C peaks were represented by acRIP/input (See details in the Method). **G**, Experimental design. Three weeks after AAV injection, the control (Ctrl) and Nat10 conditional knockout (cKO) mice were subjected to MWM training and probe test, and

then the SYN fractions were purified from hippocampal tissues for RT-qPCR and western blot analysis. **H**, The mRNA levels of Arc, Camk2α and Grin2b from the input of SYN were similar between control and Nat10 cKO mice. The RNA purified from the SYN was subjected to the RT-qPCR analysis. NS, not significant, two-tailed t-test, n = 4 biological replicates. The levels of mRNA were normalized by that of Gapdh in each sample, and then the ratio of mRNA to Gapdh were normalized by controls. **I**, The ac4C modification of Arc, Camk2α, and Grin2b mRNA was significantly reduced in the SYN of Nat10 cKO mice at day 6, compared with controls. The RNA purified from the acRIP and IgG-IP products of SYN was subjected to the RT-qPCR analysis. *** $P < 0.001$, two-way-ANOVA followed by Tukey's multiple comparison test, n = 4 biological replicates. Data were normalized by input. **J**, The protein levels of ARC, CaMK2α and GluN2B were significantly increased in the SYN of Nat10 cKO mice at day 6, compared with controls. Left, representative western blot images; right, quantification data. *** $P < 0.001$, two-tailed t-test, n = 4 biological replicates. The protein levels were normalized by that of PSD95 in each sample, and then the ratio of protein to PSD95 were normalized by controls. Quantification data are expressed as mean ± SEM.

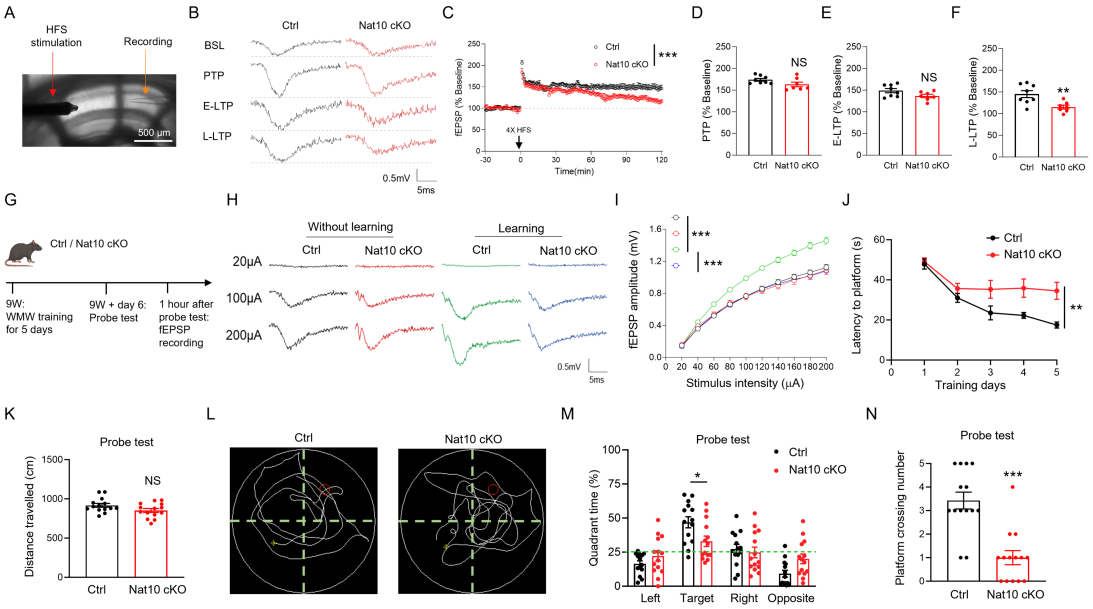

Figure 7 Impaired LTP as well as learning and memory in the Nat10 cKO mice. A, A representative image showing recording LTP at the SC-CA1 synapses from Nat10

cKO mice using the protocol of high-frequency stimulation (HFS). Scale bar, 500 μm. **B**, The representative fEPSP traces from baseline (BSL), post-tetanus potentiation (PTP), early phase of LTP (E-LTP, 55-60 min after HFS) and late phase of LTP (L-LTP, 115-120 min after HFS). **C**, Impaired maintenance of L-LTP at the SC-CA1 synapses in Nat10 cKO mice, compared with controls. Normalized fEPSP amplitudes were plotted every 1 min for hippocampal slices from control and Nat10 cKO mice. *** $P < 0.001$, two-way ANOVA, n = 8 slices from 4 mice for each group. **D**, Normal LTP induction at the SC-CA1 synapses in Nat10 cKO mice, compared to controls. The PTP in panel C was quantified. NS, not significant, two-tailed t-test. n = 8 slices from 4 mice for each group. **E**, Unaltered E-LTP at the SC-CA1 synapses in Nat10 cKO mice, compared to controls. The E-LTP in panel C was quantified. NS, not significant, two-tailed t-test. n = 8 slices from 4 mice for each group. **F**, Impaired L-LTP at the SC-CA1 synapses in Nat10 cKO mice, compared with controls. The L-LTP in panel C was quantified. ** P=0.008, two-tailed t-test. n = 8 slices from 4 mice for each group. **G**, Experimental design. The control and Nat10 cKO mice were subjected to fEPSP recording at the SC-CA1 synapses after training and probe test in the MWM. **H-I**, Learning and memory-induced enhancement of glutamatergic transmission at SC-CA1 synapses was significantly impaired in Nat10 cKO mice, compared with controls. H, Representative fEPSP traces from control and Nat10 cKO mice. I, Quantification of the fEPSP amplitudes in panel H. *** Genotype $F_{(3, 680)} = 128.2$, $P < 0.0001$, two-way ANOVA followed by Sidak's multiple comparison test, n = 18 slices from 5 mice each group. **J**, Impaired learning process in Nat10 cKO mice, compared with controls. Shown are the learning curves of control and Nat10 cKO mice in the MWM. n = 14 mice per group, ** Genotype $F_{(1, 130)} = 24.08$, ** P = 0.0014, two-way ANOVA followed by Sidak's multiple comparison test. **K**, Similar distance travelled during probe tests between control and Nat10 cKO mice. NS, not significant, two-tailed t-test, n = 14 mice per group. **L**, Representative swimming traces of control and Nat10 cKO mice during probe tests. **M**, Time spent in the target quadrant was significant reduced in Nat10 cKO groups during probe tests, compared with controls. * P = 0.0198, two-

way ANOVA followed by Sidak's multiple comparison with post hoc t-test, n = 14 mice per group. **N**, Number of platform crossing was significantly reduced in Nat10 cKO mice during probe tests, compared with controls. *** P < 0.0001, two-tailed t-test, n = 14 mice per group. Quantification data are expressed as mean ± SEM.

Supplementary Figures and Legends

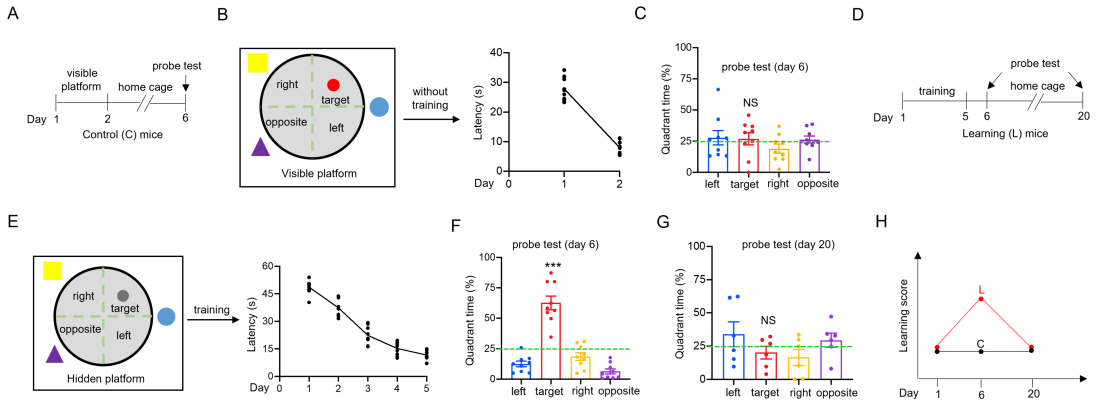

Figure S1 Protocols of Morris water maze (MWM) for control and learning mice. **A**, MWM protocol for control mice. The control mice were placed in MWM with a visible platform at days 1 and 2, after which they returned to home cage and were subjected to probe tests at day 6. **B**, Control mice were able to discern the visible platform above the water surface and consequently locate it rapidly. Shown are the latency to find the visible platform at days 1 and 2. **C**, Control mice were not able to remember the target quadrant during probe tests at day 6. Shown are the percentage of time staying in each quadrant during probe tests. NS, not significant, one-way ANOVA, n = 9 mice. **D**, MWM protocol for learning mice. The learning mice were trained in MWM with a hidden platform from day 1 to 5, and then were subjected to probe tests at day 6 and 20. **E**, Learning mice showed improvement in their ability to find the hidden platform during the training process. Shown are the learning curves. **F**, Learning mice could remember the target quadrant during probe tests at day 6. Shown are the percentage of time staying in each quadrant during probe tests. *** P < 0.001, one-way ANOVA, n = 9 mice. **G**, Learning mice could not remember the target quadrant during probe tests at day 20. Shown are the percentage of time staying in each quadrant during probe tests. NS, not significant, one-way ANOVA, n = 6 mice. **H**, Summary of learning

score of control and learning mice at days 1, 6, and 20. Memories were formed at day 6 but were forgotten at day 20.

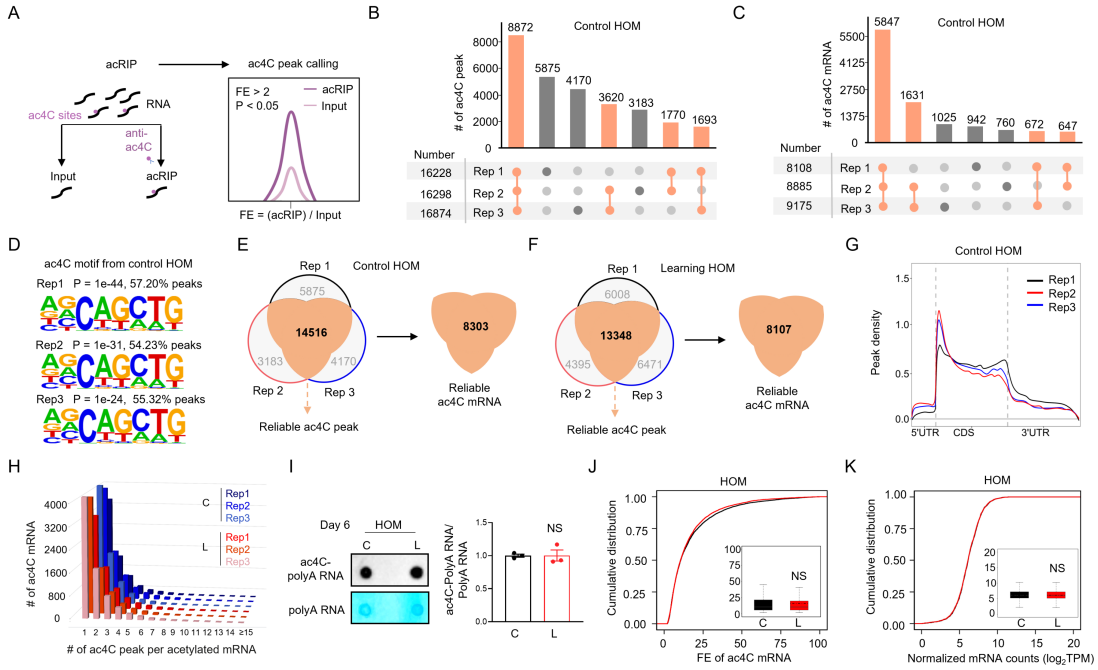

Figure S2 No significant change of total levels of ac4C mRNA in the homogenates (HOM) of mouse hippocampus after learning and memory. A, Experimental design of acRIP-seq. The RNA samples from both input and acRIP were subjected to next-generation sequencing. Among them, input was used to eliminate the background of ac4C peaks. The process of ac4C peak calling identifies reliable ac4C peaks and calculates the FE of each ac4C peak. **B**, **C**, The ac4C peaks and ac4C mRNAs are largely overlapping across the three biological replicates of control HOM samples. Shown are the number of overlapping and non-overlapping ac4C peaks (B) and ac4C mRNAs (C) across the three biological replicates of control HOM samples. **D**, The same consensus motif, AGCAGCTG, was identified in ac4C peak regions across the three biological replicates of control HOM samples. Consensus motif and its P value were generated by HOMER (see details in the Method). 99% confidence intervals: Rep 1 target 57.20%; Rep 2 target 54.23%; Rep 3 target 55.32%. **E**, **F**, Reliable ac4C peaks were those identified in at least two of the three biological replicates. Only mRNAs corresponding to these reliable ac4C peaks were defined as reliable ac4C mRNAs.

Shown are the Venn diagram of ac4C peaks for the three biological replicates of control (E) and learning (F) HOM samples. **G**, A large proportion of ac4C peaks in the HOM of mouse hippocampus are located within the CDS of mRNA. Shown are the relative density of ac4C peaks identified in different regions of transcripts for the three biological replicates of control HOM samples. CDS, coding sequence; UTRs, untranslated regions. **H**, The number of ac4C peaks for each ac4C mRNA is comparable across the three biological replicates in both control and learning HOM samples. **I**, Acetylation of polyA RNA was not altered in the HOM of mouse hippocampus after memory formation. The polyA RNA samples used for each ac4C dot-blot were 0.5 μg that falls into the linear range. The HOM polyA RNA samples of control and learning mice at day 6 after MWM training were subjected to ac4C dot-blots and methylene blue staining. Left, representative images; right, quantification data. NS, not significant, two-tailed t-test, n = 3 biological replicates at each condition. Data were normalized by controls. **J**, Acetylation of ac4C mRNA did not significantly change in the HOM of mouse hippocampus after memory formation. Shown are cumulative distribution curves of FE of ac4C mRNA in control and learning mice at day 6 after MWM training. The FE of ac4C mRNA was quantified in the quartile boxplots, where the solid line in the box is the median and the dashed line is the mean, where the maximum and minimum values are identified. NS, not significant, Kolmogorov-Smirnov test. **K,** The total mRNA levels did not significantly change in the HOM of mouse hippocampus after memory formation. Shown are cumulative distribution curves of normalized mRNA counts in the HOM of control and learning mice at day 6 after MWM training. The normalized mRNA counts of each group were quantified in the quartile boxplots, where the solid line in the box is the median and the dashed line is the mean, where the maximum and minimum values are identified. NS, not significant, Kolmogorov-Smirnov test. FE, Fold Enrichment. C, control; L, learning.

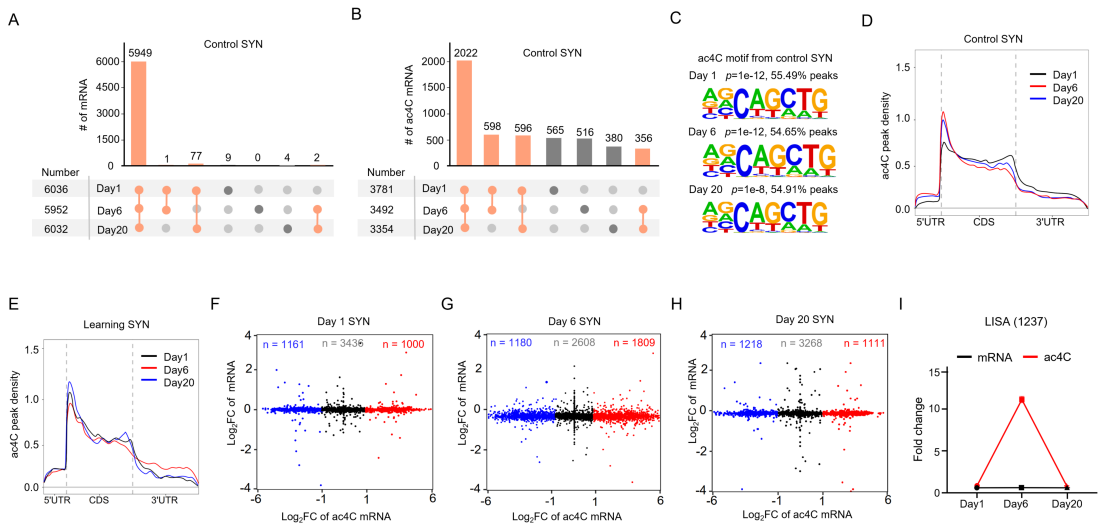

Figure S3 Identification of synaptosome (SYN) ac4C epitranscriptome and learning-induced synaptic ac4C (LISA) mRNAs in mouse hippocampus. A, **B**, The mRNA and ac4C mRNAs are largely overlapping across the SYN control group at days 1, 6, and 20. Shown are the number of overlapping and non-overlapping mRNAs (A) and ac4C mRNAs (B) across the control SYN samples at days 1, 6 and 20 after MWM training. **C**, The same consensus motif, AGCAGCTG, was identified in ac4C peak regions across the control SYN samples at days 1, 6 and 20. Consensus motif and its P value were generated by HOMER (see details in the Method). 99% confidence intervals: Day 1 target 55.49%; Day 6 target 54.65%; Day 20 target 54.91%. **D**, **E**, A large proportion of ac4C peaks in the SYN of mouse hippocampus are located within the CDS of mRNA. Shown are the relative density of ac4C peaks identified in different regions of transcripts for control (D) and learning (E) SYN samples at days 1, 6 and 20. CDS, coding sequence; UTRs, untranslated regions. **F-H**, Scatter plot showing the fold change (FC) of mRNA and ac4C mRNA in the SYN of mouse hippocampus at days 1, 6, and 20 after MWM training. The x-axis represents the $\log_2$ FC of ac4C mRNA, while the y-axis shows the $\log_2$ FC of mRNA. The red color represents upregulated ac4C mRNAs, the blue color indicates downregulated ac4C mRNAs, and the black color represents unchanged ac4C mRNAs. The cut off values for upregulation and downregulation are FC >2 and FC < 0.5, respectively. **I**, The ac4C rather than total levels of LISA mRNA are upregulated following memory formation and return to control levels after memory forgetting. The FC of total and ac4C levels for LISA mRNA

1701 were quantified at days 1, 6 and 20 after MWM training.

1702

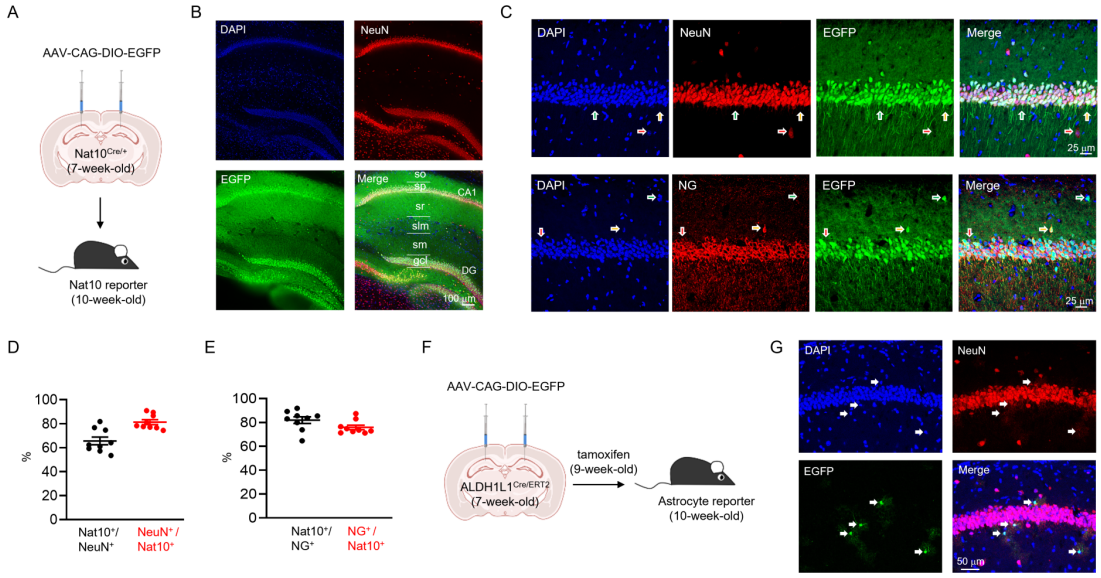

1703

1704 **Figure S4 Expression of Nat10 in the mature neurons of mouse hippocampus. A**,
1705 Experimental design. Cre-reporting AAV was injected into the dorsal hippocampus of
1706 7-week-old Nat10$^{Cre/+}$ mice. Three weeks after AAV injection, the fluorescent protein
1707 EGFP was analyzed in the Nat10 reporter mice. **B**, Co-localization of EGFP with NeuN
1708 in the hippocampus of Nat10 reporter mice. The hippocampal slices from Nat10
1709 reporter mice were immunostained with anti-NeuN antibodies. so, stratum oriens; sp,
1710 stratum pyramidale; sr, stratum radiatum; slm, stratum lacunosum-moleculare; sm,
1711 stratum moleculare; gcl, granule cell layer; DG: dentate gyrus. Scale bar, 100 μm. **C**,
1712 Co-localization of EGFP and NeuN (top images) or Neurogranin (NG) (bottom images)
1713 in the CA1 region of Nat10 reporter mice. The hippocampal slices from Nat10 reporter
1714 mice were immunostained with anti-NeuN or anti-NG antibodies. The yellow arrows
1715 indicate cells coexpressing Nat10 and NeuN or NG. The red arrows represent cells
1716 expressing NeuN or NG but not Nat10. The green arrows indicate cells expressing
1717 Nat10 but not NeuN or NG. Scale bar, 25 μm. **D**, Quantification of the percentage of
1718 NeuN-positive cells expressing Nat10 (Nat10^{+} / NeuN^{+} = 65.61 ± 3.245%) and the
1719 percentage of Nat10-positive cells expressing NeuN (NeuN^{+} / Nat10^{+} = 81.31 ±
1720 2.029%). n = 9 slices from 3 mice. **E**, Quantification of the percentage of NG-positive
1721 cells expressing Nat10 (Nat10^{+} / NG^{+} = 81.87 ± 2.765%) and the percentage of Nat10-

positive cells expressing NG (NG^+ / $Nat10^+$ = 75.82 ± 1.882%). n = 9 slices from 3 mice. **F**, Experimental design. Cre-reporting AAV was injected into the dorsal hippocampus of 7-week-old $ALDH1L1^{Cre/ERT2}$ mice. Three weeks after AAV injection, the fluorescent protein EGFP was analyzed in the astrocyte reporter mice. **G**, Astrocytes in the CA1 region of astrocyte reporter mice do not co-localize with NeuN (white arrow). The hippocampal slices from astrocyte reporter mice were immunostained with anti-NeuN antibodies. Scale bar, 50 μm.

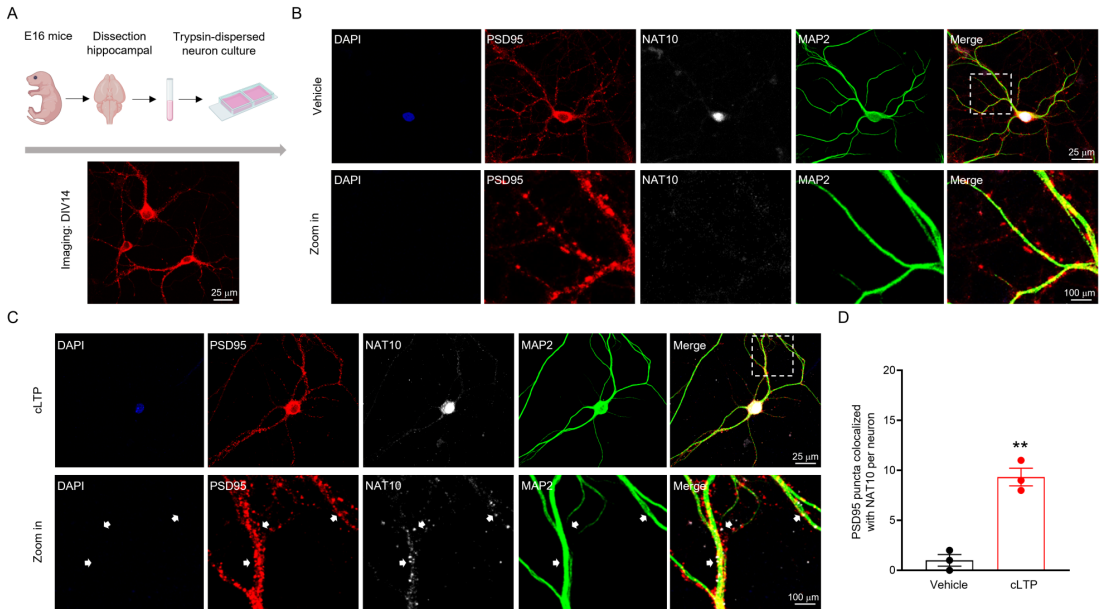

Figure S5 Increased colocalization of NAT10 and PSD95 in cultured mouse hippocampal neurons after cLTP stimulation. A, Experimental design. The primary neurons were taken from the E16 mouse hippocampus, and the immunostaining was performed at DIV 14. **B**, Fluorescent images of DAPI, PSD95, NAT10 and MAP2 in cultured hippocampal neurons treated with vehicle. The bottom images were enlarged from the rectangle in the top images. Scale bar, 25 μm (top) and 100 μm (bottom). C, Fluorescent images of DAPI, PSD95, NAT10 and MAP2 in cultured hippocampal neurons 60 min after cLTP stimulation. The bottom images were enlarged from the rectangle in the top images. Scale bar, 25 μm (top) and 100 μm (bottom). **D**, Increased colocalization of NAT10 and PSD95 in the dendrites of cultured hippocampal neurons. The number of PSD95 puncta colocalized with NAT10 was quantified. ** P = 0.0014,

two-tailed t-test, n = 30 neurons from 3 independent experiments. DIV, days in vitro. DAPI, a nuclear marker; PSD95, a protein marker for postsynaptic density; MAP2 (microtubule-associated protein 2), a protein marker for soma and dendrites.

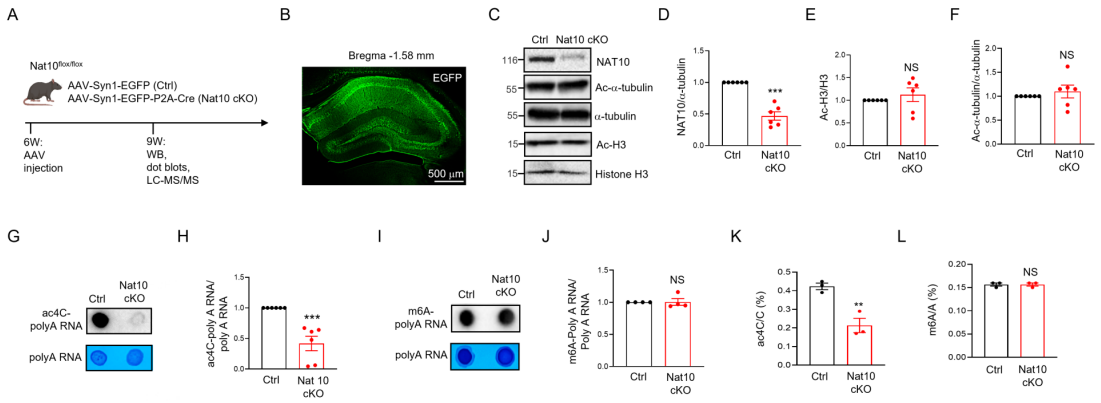

Figure S6 NAT10-dependent ac4C modification of polyA RNA in mouse hippocampus. A, Experimental design. Three weeks after AAV injection, the homogenates of hippocampal tissues from control (Ctrl) and Nat10 cKO mice were collected for western blots, ac4C and m6A dot-blots, and LC-MS/MS analysis. **B**, Infection of AAV-Syn1-EGFP-P2A-Cre in the hippocampus of 9-week-old mice. Shown are fluorescent images of the mouse hippocampus expressing EGFP. Scale bar, 500 μm. **C-F**, Downregulation of NAT10, rather than acetylated tubulin or histone H3 proteins in the hippocampus of Nat10 cKO mice, compared with controls. The protein samples from control and Nat10 cKO mouse hippocampus were probed with the indicated antibodies. C, representative western blot images, D-F, Quantification of NAT10/tubulin, acetylated-tubulin/tubulin and acetylated-H3/H3 in panel C. NS, not significant, *** $P < 0.0001$, two-tailed t-test, n = 6 biological replicates. Data were normalized by controls. **G-H**, Reduced ac4C modification of polyA RNA in the hippocampus of Nat10 cKO mice, compared with controls. The polyA RNA samples purified from mouse hippocampus were subjected to ac4C dot-blots and methylene blue staining. G, Representative images. H, Quantification data. *** $P = 0.0006$, two-tailed t-test, n = 6 biological replicates. Data were normalized by controls. **I-J**, Similar m6A modification of polyA RNA in the hippocampus of control and Nat10 cKO mice. I, Representative images. J, Quantification data. NS, not significant, two-tailed t-test, n =

4 biological replicates. **K**, Reduced ac4C modification of polyA RNA in the hippocampus of Nat10 cKO mice, compared with controls. The stoichiometry levels of ac4C from LC-MS/MS analysis were quantified. ** P = 0.0077, two-tailed t-test, n = 3 biological replicates. **L**, Similar m6A modification of polyA RNA in the hippocampus of control and Nat10 cKO mice. The stoichiometry levels of m6A from LC-MS/MS analysis were quantified. NS, not significant, two-tailed t-test, n = 3 biological replicates.

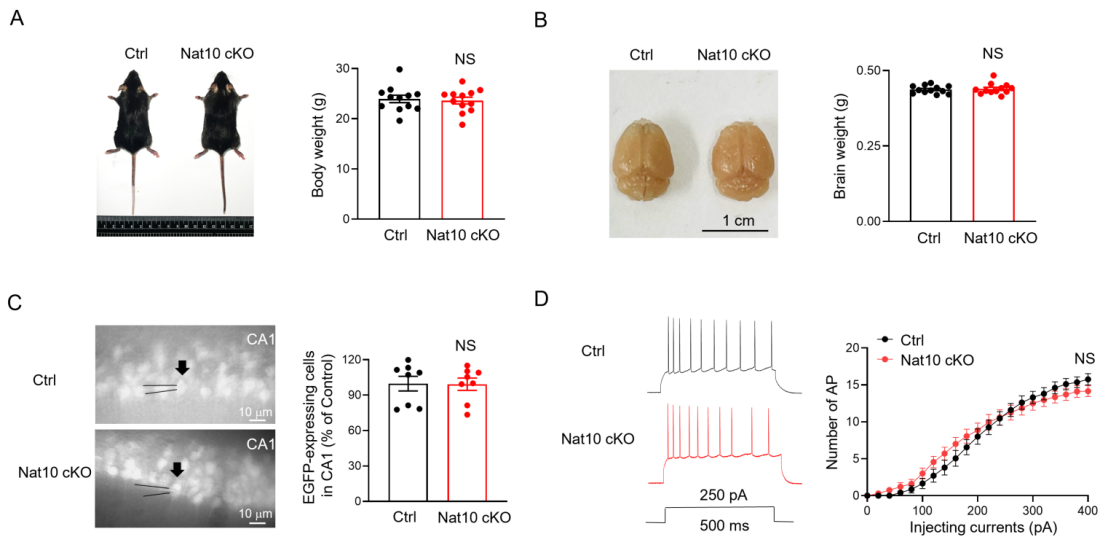

Figure S7 Downregulation of NAT10 in mouse hippocampus does not affect body or brain weight, neuronal number or intrinsic excitability. A, Similar body weight between 10-week-old control and Nat10 cKO mice. Left, representative images of the mice, right, quantification of body weight. NS, not significant, two-tailed t-test, n = 12 mice for each group. **B**, Similar brain weight between 10-week-old control and Nat10 cKO mice. Left, representative images of mouse brain, right, quantification of brain weight. NS, not significant, two-tailed t-test, n = 12 mice for each group. **C**, Similar number of neurons expressing EGFP in the CA1 region of 10-week-old control and Nat10 cKO mice. Left, representative images of CA1 neurons expressing EGFP, right, quantification of EGFP-expressing cells in the CA1 region. NS, not significant, two-tailed t-test, n = 8 slices from 4 mice for each group. Data were normalized by control. **D**, Similar intrinsic excitability of CA1 pyramidal neurons between 10-week-old

control and Nat10 cKO mice. Left, representative traces of action potentials (AP) of CA1 pyramidal neurons; right, quantification of AP number after injection of different currents into CA1 pyramidal neurons. NS, not significant, two-way ANOVA followed by Sidak's multiple comparison test, n = 20 cells from 4 mice for each group.

Supplementary Tables and Legends

Table S1. Library Information of acRIP-seq.

Table S2. List of mRNAs identified by regular acRIP-seq (HOM).

Table S3. List of mRNAs identified by low-input acRIP-seq (SYN).

Table S4. The information of LISA mRNA.

Table S5. The information of NASA mRNA.